EUROPEAN ORGANIZATION FOR NUCLEAR RESEARCH (CERN)

FERMILAB-PUB-13-638-CMS

CERN-PH-EP/2013-108
2013/09/02

CMS-EWK-11-009

Measurement of the Wγ and Zγ inclusive cross sections in pp collisions at $\sqrt{s} = 7\,\text{TeV}$ and limits on anomalous triple gauge boson couplings

The CMS Collaboration*

Abstract

Measurements of Wγ and Zγ production in proton-proton collisions at $\sqrt{s} = 7\,\text{TeV}$ are used to extract limits on anomalous triple gauge couplings. The results are based on data recorded by the CMS experiment at the LHC that correspond to an integrated luminosity of $5.0\,\text{fb}^{-1}$. The cross sections are measured for photon transverse momenta $p_{\text{T}}^{\gamma} > 15\,\text{GeV}$, and for separations between photons and final-state charged leptons in the pseudorapidity-azimuthal plane of $\Delta R(\ell,\gamma) > 0.7$ in $\ell\nu\gamma$ and $\ell\ell\gamma$ final states, where ℓ refers either to an electron or a muon. A dilepton invariant mass requirement of $m_{\ell\ell} > 50\,\text{GeV}$ is imposed for the Zγ process. No deviations are observed relative to predictions from the standard model, and limits are set on anomalous WWγ, ZZγ, and Z$\gamma\gamma$ triple gauge couplings.

Submitted to Physical Review D

*See Appendix A for the list of collaboration members

1 Introduction

The standard model (SM) has been enormously successful in describing the electroweak (EW) and strong interactions. However, important questions remain unanswered regarding possible extensions of the SM that incorporate new interactions and new particles. The self-interactions of the electroweak gauge bosons comprise an important and sensitive probe of the SM, as their form and strength are determined by the underlying $SU(2) \times U(1)$ gauge symmetry. A precise measurement of the production of pairs of EW bosons ("diboson" events) provides direct information on the triple gauge couplings (TGCs), and any deviation of these couplings from their SM values would be indicative of new physics. Even if the new phenomena involve the presence of objects that can only be produced at large energy scales, i.e., beyond the reach of the Large Hadron Collider (LHC), they can nevertheless induce changes in the TGCs. In addition, since diboson processes represent the primary background to the SM Higgs production, their precise measurement is important for an accurate evaluation of Higgs boson production at the LHC, particularly in association with gauge bosons.

Aside from $\gamma\gamma$ production, the EW Wγ and Zγ production processes at hadron colliders provide the largest and cleanest yields, as backgrounds to Wγ and Zγ production can be significantly suppressed through the identification of the massive W and Z vector bosons via their leptonic decay modes. Measurements from LEP [1–4], the Tevatron [5–9], and from initial analyses at the LHC [10–12] have already explored some of the parameter space of anomalous TGCs (ATGCs) in Wγ and Zγ processes.

We describe an analysis of inclusive Wγ and Zγ events, collectively referred to as "Vγ" production, based on the leptonic decays $W \to e\nu$, $W \to \mu\nu$, $Z \to ee$, and $Z \to \mu\mu$, observed in pp collisions at a center-of-mass energy of 7 TeV. The data, corresponding to an integrated luminosity $L = 5.0\,fb^{-1}$, were collected in 2011 with the Compact Muon Solenoid (CMS) detector at the LHC. The previous results from pp collisions at $\sqrt{s} = 7$ TeV at the LHC were limited by the statistics of the data samples, and this analysis achieves a significant improvement in precision.

Vγ production can be represented by the Feynman diagrams of Fig. 1. Three processes contribute: (a) initial-state radiation, where a photon is radiated by one of the incoming virtual partons, (b) final-state radiation, where a photon is radiated by one of the charged leptons from V decay, and (c) TGC at the WWγ vertex in Wγ production, and the ZZγ and Z$\gamma\gamma$ vertices in Zγ production. In the SM, contributions from the TGC process are expected only for Wγ production, because neutral TGCs are forbidden at tree level [13, 14].

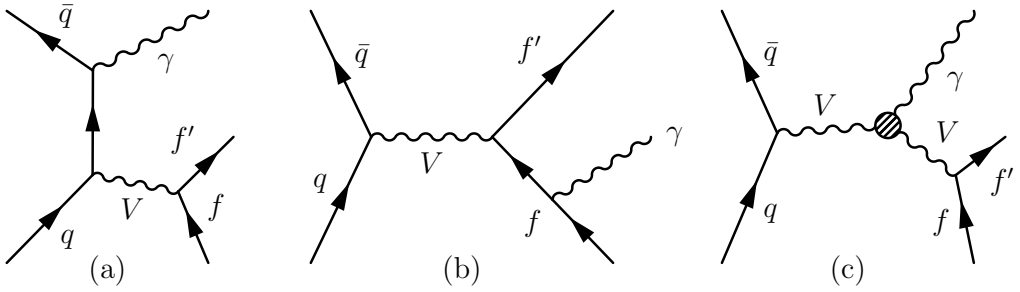

Figure 1: The three lowest order diagrams for Vγ production, with V corresponding to both virtual and on-shell γ, W, and Z bosons. The three diagrams reflect contributions from (a) initial-state and (b) final-state radiation and (c) TGC. The TGC diagram does not contribute at the lowest order to SM Zγ production since photons do not couple to particles without electric charge.

This paper is organized as follows. Brief descriptions of the CMS detector and Monte Carlo (MC) simulations are given in Section 2. Selection criteria used to identify the final states are given in Section 3. Dominant backgrounds to Vγ production are described in Section 4, along with methods used to estimate background contributions. Measurements of cross sections and limits on ATGCs are given, respectively, in Section 5 and 6, and the results are summarized in Section 7.

2 CMS detector and Monte Carlo simulation

The central feature of the CMS apparatus is a superconducting solenoid, which is 13 m long and 6 m in diameter, and provides an axial magnetic field of 3.8 T. The bore of the solenoid is instrumented with detectors that provide excellent performance for reconstructing hadrons, electrons, muons, and photons. Charged particle trajectories are measured with silicon pixel and strip trackers that cover all azimuthal angles $0 < \phi < 2\pi$ and pseudorapidities $|\eta| < 2.5$, where η is defined as $-\ln[\tan(\theta/2)]$, with θ being the polar angle of the trajectory of the particle relative to the counterclockwise-beam direction. A lead tungstate crystal electromagnetic calorimeter (ECAL) and a brass/scintillator hadron calorimeter (HCAL) surround the tracking volume. Muons are identified and measured in gas-ionization detectors embedded in the steel flux return yoke outside of the solenoid. The detector coverage is nearly hermetic, providing thereby accurate measurements of the imbalance in momentum in the plane transverse to the beam direction. A two-tier trigger system selects the most interesting pp collisions for use in analyses. A more detailed description of the CMS detector can be found in Ref. [15].

The main background to Wγ and Zγ production arises from W+jets and Z+jets events, respectively, in which one of the jets is misidentified as a photon. To minimize systematic uncertainties associated with the modeling of parton fragmentation through MC simulation, this background is estimated from multijet events in data, as described in Section 4. The background contributions from other processes, such as $\mathrm{t\bar{t}}$, γ+jets, and multijet production, are relatively small, and are estimated using MC simulation.

The MC samples for the signal processes W$\gamma + n$ jets and Z$\gamma + n$ jets, where $n < 3$, are generated with MADGRAPH v5.1.4.2 [16] and interfaced to PYTHIA v6.424 [17] for parton showering and hadronization. The kinematic distributions for these processes are cross-checked with expectations from SHERPA v1.2.2 [18], and the predictions from the two programs are found to agree. The signal samples are normalized to the predictions of next-to-leading-order (NLO) quantum chromodynamics from the MCFM v6.5 generator [19, 20] using the CTEQ6.6 NLO parton distribution functions (PDF) [21].

Backgrounds from $\mathrm{t\bar{t}}$, W+jets, Z+jets, WW, and $\gamma\gamma$ events are also simulated with the MADGRAPH program interfaced with PYTHIA. Multijet, γ+jets, and WZ and ZZ diboson events are generated using the stand-alone PYTHIA MC program, and have negligible impact on the analysis. All these MC event samples, generated using the CTEQ6L1 leading-order (LO) PDF [22], are passed through a detailed simulation of the CMS detector based on GEANT4 [23], and reconstructed with the same software that is used for data.

3 Selection of candidate events

The requirements for selecting isolated muons follow closely the standard CMS muon identification criteria [24]. However, electron and photon selection criteria are optimized specifically for this analysis, and are described in greater detail in the following subsections, as are the re-

construction of transverse momentum imbalance or the "missing" transverse momentum ($\not\!\!E_T$), all trigger requirements, and the selections used to enhance the purity of signal.

The presence of pileup from additional overlapping interactions is taken into account in the analysis, and cross-checked by studying the effectiveness of the selection criteria, separately, for small and large pileup rates in data. There are on average 5.8 overlapping interactions per collision for low-pileup data, and 9.6 interactions for high-pileup data, which correspond, respectively, to integrated luminosities of $L \approx 2.2\,fb^{-1}$ (referred to subsequently as Run 2011A) and to $L \approx 2.7\,fb^{-1}$ (referred to as Run 2011B).

3.1 Electron identification and selection

Electrons are identified as "superclusters" (SC) of energy deposition [25] in the ECAL fiducial volume that are matched to tracks from the silicon tracker. Tracks are reconstructed using a Gaussian-sum filter algorithm that takes into account possible energy loss due to bremsstrahlung in the tracker. The SC are required to be located within the acceptance of the tracker ($|\eta| < 2.5$). Electron candidates in the transition regions between the central barrel (EB) and the endcap (EE) sections of the ECAL ($1.4442 < |\eta| < 1.566$) have reduced efficiency, and are therefore excluded. The reconstructed electron tracks are required to have hits observed along their trajectories in all layers of the inner tracker. Electron candidates must have $p_T > 35$ and $>20\,GeV$ for the Wγ and Zγ analyses, respectively.

Particles misidentified as electrons are suppressed through the use of an energy-weighted width quantity in pseudorapidity ($\sigma_{\eta\eta}$) that reflects the dispersion of energy in η ("shower shape") in a 5×5 matrix of the 25 crystals centered about the crystal containing the largest energy in the SC [25]. The $\sigma_{\eta\eta}$ parameter is defined through a mean $\bar{\eta} = \sum \eta_i w_i / \sum w_i$ as follows:

$$\sigma_{\eta\eta}^2 = \frac{\sum (\eta_i - \bar{\eta})^2 w_i,}{\sum w_i}, i = 1, \ldots, 25, \tag{1}$$

where the sum runs over all the elements of the 5×5 matrix, and $\eta_i = 0.0174\hat{\eta}_i$, with $\hat{\eta}_i$ denoting the η index of the ith crystal; the individual weights w_i are given by $4.7 + \ln(E_i/E_T)$, unless any of the w_i are found to be negative, in which case they are set to zero. In the ensuing analysis, the value of $\sigma_{\eta\eta}$ is required to be consistent with expectations for electromagnetic showers, and the discriminant is used to suppress background as well as to assess contribution from signal and background in fits to the data discussed in Section 4.1.1.

In addition, the η and ϕ coordinates of the track trajectories extrapolated to the ECAL are required to match those of the SC, and limits are imposed on the amount of HCAL energy deposited within a cone of $\Delta R < 0.15$ relative to the axis of the ECAL cluster. To reduce background from $\gamma \to e^+e^-$ conversions in the tracker material, the electron candidates are required to have no "partner" tracks within 2 mm of the extrapolated point in the transverse plane where both tracks are parallel to each other (near the hypothesized point of the photon conversion), and the difference in the cotangents of their polar angles must satisfy $|\Delta \cot\theta| > 0.02$. To ensure that an electron trajectory is consistent with originating from the primary interaction vertex, taken to be the one with the largest scalar sum of the p_T^2 of its associated tracks in the case of multiple vertices, the distances of closest approach are required to be $|d_z| < 0.1\,cm$ and $|d_T| < 0.02\,cm$ for the longitudinal and transverse coordinates, respectively.

To reduce background from jets misidentified as electrons, the electron candidates are required to be isolated from other energy depositions in the detector. The electron selection criteria are

obtained by optimizing signal and background levels using simulated samples. This optimization is done separately for the EB and EE sections. Different criteria are used for the $W\gamma \to e\nu\gamma$ and $Z\gamma \to ee\gamma$ channels because of the different trigger requirements and relative background levels. For the $Z\gamma$ analysis, a relative isolation parameter (I_r) is calculated for each electron candidate through a separate sum of scalar p_T in the ECAL, HCAL, and tracker (TRK), all defined relative to the axis of the electron, but without including its p_T, within the spatial cone $\Delta R = \sqrt{(\Delta\phi)^2 + (\Delta\eta)^2} < 0.3$. This sum, reduced by $\rho \times \pi \times 0.3^2$ to account for the pileup contributions to the isolation parameter, and divided by the p_T of the electron candidate, defines the I_r for each subdetector. Here ρ is the mean energy (in GeV) per unit area of (η, ϕ) for background from pileup, computed event by event using the FASTJET package [26].

The $W\gamma$ analysis uses individual I_r contributions from the three subdetectors. Also, to minimize the contributions from $Z\gamma$ events, a less restrictive selection is applied to the additional electron. The efficiencies for these criteria are measured in $Z \to ee$ data and in MC simulation, using the "tag-and-probe" technique of Ref. [27]. An efficiency correction of ≈3% is applied to the MC simulation to match the performance observed in data.

3.2 Photon identification and selection

Photon candidates in the fiducial volume of the ECAL detector are reconstructed as SC with efficiencies very close to 100% for $p_T^\gamma > 15\,\text{GeV}$, as estimated from MC simulation. The photon energy scale is measured using $Z \to \mu\mu\gamma$ events, following the "PHOSPHOR" procedure described in Ref. [28].

As in the previous CMS analysis of $V\gamma$ final states [11], we reduce the rate of jets misreconstructed as photons by using stringent photon identification criteria, including isolation and requirements on shapes of electromagnetic (EM) showers. In particular, (i) the ratio of HCAL to ECAL energies deposited within a cone of $\Delta R = 0.15$ relative to the axis of the seed ECAL crystal must be < 0.05, (ii) the value of $\sigma_{\eta\eta}$ must be < 0.011 in the barrel and < 0.030 in the endcap, and (iii) to reduce background from misidentified electrons, photon candidates must have no associated tracks in the pixel detector.

However, unlike in the previous analysis [11], the pileup conditions during Run 2011 require modifications to photon isolation criteria to achieve reliable modeling of pileup effects. The scalar sum of transverse momenta of all the tracks found in the annulus $0.05 < \Delta R < 0.4$ around each photon candidate is therefore required to have $p_T^{TRK} < 2\,\text{GeV} + 0.001 \times p_T^\gamma + A_{\text{eff}} \times \rho$, where A_{eff} is the effective area used to correct each photon shower for pileup. This procedure ensures that the isolation requirement does not exhibit a remaining dependence on pileup. For each photon candidate, the scalar sum of the p_T deposited in the ECAL in an annulus $0.06 < \Delta R < 0.40$, excluding a rectangular strip of $\Delta\eta \times \Delta\phi = 0.04 \times 0.40$ to reduce the impact of energy leakage from any converted $\gamma \to e^+e^-$ showers, is computed. The isolation in the ECAL is required to have $p_T^{ECAL} < 4.2\,\text{GeV} + 0.006 \times p_T^\gamma + A_{\text{eff}} \times \rho$, and, finally, the isolation criterion in the HCAL is $p_T^{HCAL} < 2.2\,\text{GeV} + 0.0025 \times p_T^\gamma + A_{\text{eff}} \times \rho$. The expected values of A_{eff} are defined by the ratio of slopes obtained in fits of the isolation and ρ parameters to a linear dependence on the number of vertices observed in data. These are summarized in Table 1, separately for the three isolation parameters, calculated for EM showers observed in the barrel and endcap regions of the ECAL.

To estimate the efficiency of requirements on the shape and isolation of EM showers, we use the similarity between photon and electron showers and a tag-and-probe technique in which one of the electrons from $Z \to ee$ decay is required to pass more stringent electron criteria, to check whether its partner electron satisfies the photon selection criteria when the requirement

Table 1: The values of A_{eff}, in units of $\Delta\eta \times \Delta\phi$, used to correct contributions from pileup to the summed p_{T} accompanying photon candidates in the tracker and the two calorimeters, separately for photons observed in the barrel and endcap regions of the ECAL.

Isolation	Barrel	Endcap
Tracker	0.0167	0.032
ECAL	0.183	0.090
HCAL	0.062	0.180

of not having a hit in the pixel detector is ignored. The results for data and MC simulation, as a function of p_{T}^{γ} and η^{γ}, are shown in Fig. 2. The efficiencies obtained using generator-level information in $\text{Z} \to \text{ee}$ and in γ+jets simulations are also shown in Fig. 2. The difference between these efficiencies is taken as an estimate of systematic uncertainty in the photon-identification efficiency, based on results from $\text{Z} \to \text{ee}$ data. The ratios of efficiency in data to that in simulation, both measured by the tag-and-probe method (squares), and efficiency in $\text{Z} \to \text{ee}$ simulation to that in the γ+jets simulation obtained from generator-level information (triangles), as a function of p_{T}, integrated over the full range of η, are shown in Fig. 3. We find that the efficiencies in data and MC simulation agree to within 3% accuracy. As for the case of electrons and muons, we reweight the simulated events to reduce the residual discrepancy in modeling efficiency as a function of p_{T}^{γ} and η^{γ}.

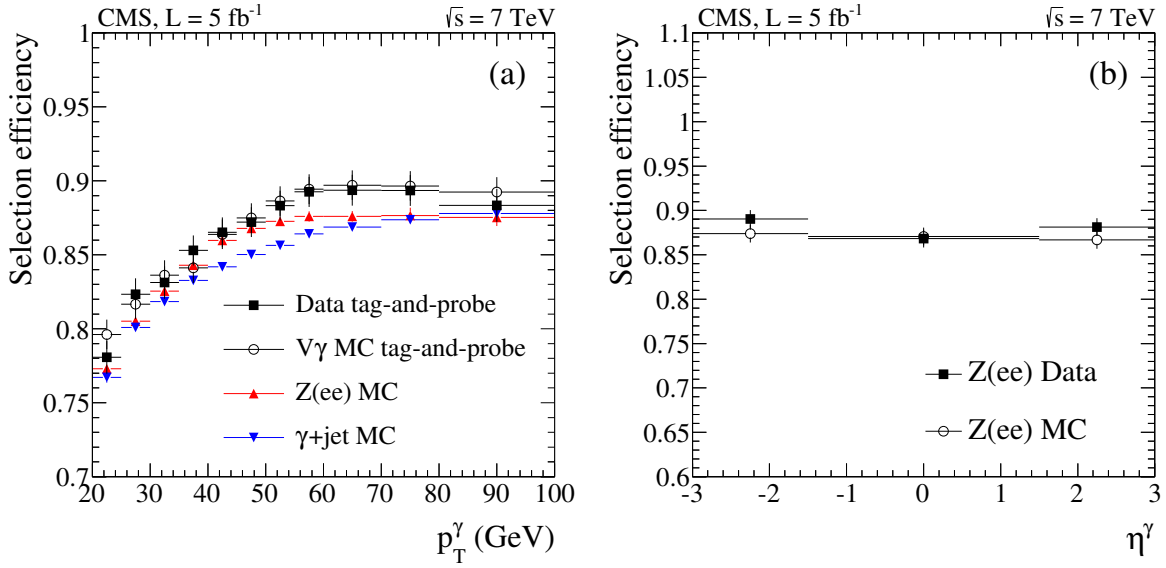

Figure 2: Efficiency of photon selection, as a function of (a) photon transverse momentum and (b) photon pseudorapidity.

The efficiency of the pixel veto is obtained from $\text{Z} \to \mu\mu\gamma$ data, where the photon arises from final-state radiation. The purity of such photon candidates is estimated to exceed 99.6%, and they are therefore chosen for checking photon-identification efficiency, energy scale, and energy resolution. We find that the efficiency of the pixel veto corresponds to 97% and 89% for photons in the barrel and endcap regions of the ECAL, respectively.

3.3 Muon identification and selection

Muons are reconstructed offline by matching particle trajectories in the tracker and the muon system. The candidates must have $p_{\text{T}} > 35$ and $> 20\,\text{GeV}$ for the $\text{W}\gamma$ and $\text{Z}\gamma$ analyses, respectively. We require muon candidates to pass the standard CMS isolated-muon selection

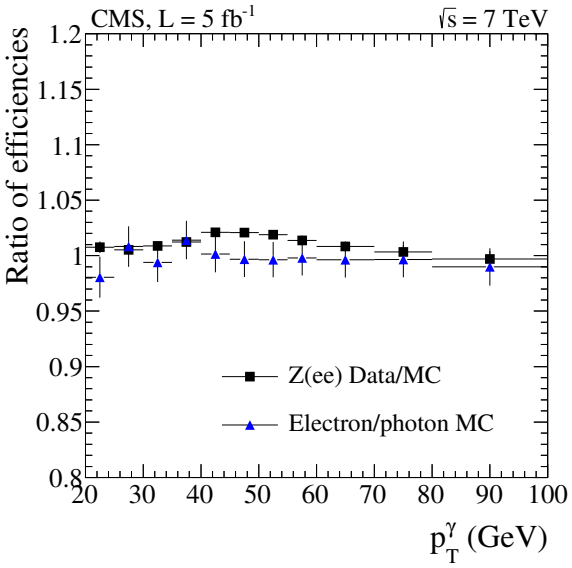

Figure 3: Ratio of efficiencies for selecting photons in data relative to MC simulation, obtained through the tag-and-probe method, and the ratio of electron to photon efficiencies, obtained at the MC generator level, with both sets of ratios given as a function of the transverse momentum of the photon.

criteria [24], with minor changes in requirements on the distance of closest approach of the muon track to the primary vertex. We require $|d_z| < 0.1$ cm, in the longitudinal direction, and $|d_T| < 0.02$ cm, in the transverse plane. The efficiencies for these criteria are measured in data and in MC simulation using a tag-and-probe technique applied to $Z \to \mu\mu$ events. An efficiency correction of ≈3% is also applied to the MC simulation to match the performance found in muon data.

3.4 Reconstruction of E_T

Neutrinos from $W \to \ell\nu$ decay are not detected directly, but give rise to an imbalance in reconstructed transverse momentum in an event. This quantity is computed using objects reconstructed with the particle-flow algorithm [29], which generates a list of four-vectors of particles based on information from all subsystems of the CMS detector. The $\not{E}_T$ for each event is defined by the magnitude of the vector sum of the transverse momenta of all the reconstructed particles.

3.5 Trigger requirements

The $W\gamma \to \ell\nu\gamma$ and $Z\gamma \to \ell\ell\gamma$ events are selected using unprescaled, isolated-lepton triggers. The p_T thresholds and isolation criteria imposed on lepton candidates at the trigger level changed with time to accommodate the instantaneous luminosity, and are less stringent than the offline requirements.

For the $W\gamma \to e\nu\gamma$ channel, we use an isolated, single-electron trigger, requiring electrons with $|\eta| < 3$, and a p_T threshold of 32 GeV, except for the first part of Run 2011A ($L = 0.2\,fb^{-1}$), where the threshold is 27 GeV. In addition, for the last part ($L = 1.9\,fb^{-1}$) of Run 2011A and the entire Run 2011B, a selection is implemented on the transverse mass (M_T^W) of the system consisting of the electron candidate and the $\not{E}_T$, requiring $M_T^W = \sqrt{2p_T^\ell \not{E}_T(1-\cos\Delta\phi(\ell,\not{E}_T))} > 50$ GeV, where $\Delta\phi$ is the angle between the p_T^ℓ and the $\not{E}_T$ vectors. The trigger used for the $Z\gamma \to ee\gamma$

events requires two isolated electron candidates with p_T thresholds of 17 GeV on the leading (highest-p_T) candidate and 8 GeV on the trailing candidate.

The trigger for $W\gamma \to \mu\nu\gamma$ events requires an isolated muon with $p_T > 30$ GeV and $|\eta| < 2.1$. The dimuon trigger used to collect $Z\gamma \to \mu\mu\gamma$ events does not require the two muons to be isolated, and has coverage for $|\eta| < 2.4$. For most of the data, the muon p_T thresholds are 13 GeV for the leading and 8 GeV for the trailing candidates. For the first part of Run 2011A (L = 0.2 fb^{-1}) and for most of the remaining data, these thresholds are 7 GeV for each muon candidate, except for the last part of Run 2011B (L = 0.8 fb^{-1}), where these increase to 17 and 8 GeV, respectively.

3.6 Wγ event selections

The $W\gamma \to \ell\nu\gamma$ process is characterized by a prompt, energetic, and isolated lepton, a prompt isolated photon, and significant $\not{E}_T$ that reflects the escaping neutrino. Both electrons and muons are required to have $p_T > 35$ GeV, and photons to have $p_T > 15$ GeV. The maximum allowed $|\eta|$ values for electrons, photons, and muons are 2.5, 2.5, and 2.1, respectively. We require the photon to be separated from the lepton by $\Delta R(\ell, \gamma) > 0.7$. To minimize contributions from $Z\gamma \to \ell\ell\gamma$ production, we reject events that have a second reconstructed lepton of the same flavor. This veto is implemented only for electrons that have $p_T > 20$ GeV, $|\eta| < 2.5$, and pass looser electron selections, and for muons that have $p_T > 10$ GeV and $|\eta| < 2.4$.

To suppress background processes without genuine $\not{E}_T$, we require events to have $M_T^W > 70$ GeV. We find that the simulation of the distribution in $\not{E}_T$ is well modeled, but we apply a small efficiency correction to reduce the residual disagreement. The efficiencies of the M_T^W selection in data and simulation agree at the 1% level. The full set of $\ell\nu\gamma$ selections yield 7470 electron and 10 809 muon candidates in the data. The selection criteria used to define the Wγ sample are summarized in Table 2.

3.7 Zγ event selections

Accepted Zγ events are characterized by two prompt, energetic, and isolated leptons, and an isolated prompt photon. Both electrons and muons are required to have $p_T > 20$ GeV, and the photons to have $p_T > 15$ GeV. The maximum $|\eta|$ values for accepted electrons, photons, and muons are 2.5, 2.5, and 2.4, respectively. We require photons to be separated from leptons by imposing a $\Delta R(\ell, \gamma) > 0.7$ requirement. Finally, the invariant mass of the two leptons is required to satisfy $m_{\ell\ell} > 50$ GeV. Applying all these selections yields 4108 $Z\gamma \to ee\gamma$ and 6463 $Z\gamma \to \mu\mu\gamma$ candidates. The selection criteria used to define the Zγ sample are summarized in Table 2.

Table 2: Summary of selection criteria used to define the Wγ and Zγ samples.

Selection	$W\gamma \to e\nu\gamma$	$W\gamma \to \mu\nu\gamma$	$Z\gamma \to ee\gamma$	$Z\gamma \to \mu\mu\gamma$
Trigger	single electron	single muon	dielectron	dimuon
p_T^ℓ (GeV)	>35	>35	>20	>20
$\|\eta^\ell\|$	EB or EE	<2.1	EB or EE	<2.4
p_T^γ (GeV)	>15	>15	>15	>15
$\|\eta^\gamma\|$	EB or EE	EB or EE	EB or EE	EB or EE
$\Delta R(\ell, \gamma)$	>0.7	>0.7	>0.7	>0.7
M_T^W (GeV)	>70	> 70		
$m_{\ell\ell}$ (GeV)			>50	>50
Other criterion	only one lepton	only one lepton		

4 Background estimates

The dominant background for both Wγ and Zγ production arises from events in which jets, originating mostly from W+jets and Z+jets events, respectively, are misidentified as photons. We estimate the background from these sources as a function of p_{T}^{γ} using the two methods described in Section 4.1.

For the Wγ channel, a second major background arises from Drell–Yan ($\mathrm{q\bar{q}} \to \ell^{+}\ell^{-}$) and EW diboson production, when one electron is misidentified as a photon. This background is estimated from data as described in Section 4.2.

Other backgrounds to Vγ processes include (i) jets misidentified as leptons in γ+jet production, (ii) Vγ events, with V decaying into $\tau\nu$ or $\tau\tau$, and subsequently $\tau \to \ell\nu\nu$, (iii) $\mathrm{t\bar{t}}\gamma$ events, and (iv) Zγ events, where one of the leptons from Z decay is not reconstructed properly. All these backgrounds are small relative to the contribution from V+jets, and are estimated using MC simulation.

4.1 Jets misidentified as photons

4.1.1 Template method

The template method relies on a maximum-likelihood fit to the distribution of $\sigma_{\eta\eta}$ in data to estimate the background from misidentified jets in the selected Vγ samples. The fit makes use of the expected distributions ("templates") for genuine photons and misidentified jets. For isolated prompt photons, the $\sigma_{\eta\eta}$ distribution is very narrow and symmetric, while for photons produced in hadron decays, the $\sigma_{\eta\eta}$ distribution is asymmetric, with a slow falloff at large values. The distribution in $\sigma_{\eta\eta}$ for signal photons is obtained from simulated Wγ events. The $\sigma_{\eta\eta}$ distribution of electrons from Z boson decays in data is observed to be shifted to smaller values relative to simulated events. The shift is 0.9×10^{-4} and 2.0×10^{-4} for the EB and EE regions, respectively, and corresponds to 1% and 0.8% shifts in the average of the simulated photon $\sigma_{\eta\eta}$ values, which are corrected for the shift relative to data.

The $\sigma_{\eta\eta}$ templates for background are defined by events in a background-enriched isolation sideband of data. These photon candidates are selected using the photon identification criteria described in Section 3.2, but without the $\sigma_{\eta\eta}$ selection, and with inverted TRK isolation requirements: (i) $2\,\mathrm{GeV} < p_{\mathrm{T}}^{\mathrm{TRK}} - 0.001 \times p_{\mathrm{T}}^{\gamma} - 0.0167 \times \rho < 5\,\mathrm{GeV}$, for $|\eta_{\gamma}| < 1.4442$, and (ii) $2\,\mathrm{GeV} < p_{\mathrm{T}}^{\mathrm{TRK}} - 0.001 \times p_{\mathrm{T}}^{\gamma} - 0.0320 \times \rho < 3\,\mathrm{GeV}$, for $1.566 < |\eta_{\gamma}| < 2.5$. These requirements ensure that the contributions from genuine photons are negligible, while the isolation requirements remain close to those used for selection of photons and thereby provide jets with large EM energy fractions that have properties similar to those of genuine photons. We observe that $\sigma_{\eta\eta}$ is largely uncorrelated with the isolation parameter in simulated multijet events, so that the distribution observed for background from jets that are misidentified as photons (i.e., with inverted tracker isolation criteria) is expected to be the same as that for jets misidentified as isolated photons.

Because of the $M_{\mathrm{T}}^{\mathrm{W}}$ requirement in selected Wγ events, the presence of significant $\not\!\!E_{\mathrm{T}}$ can bias the estimation of the background. We therefore investigate possible correlations between the distribution in $\sigma_{\eta\eta}$ for background events and the projection of $\not\!\!E_{\mathrm{T}}$ along the p_{T} of jets misidentified as photons. In particular, we define $\sigma_{\eta\eta}$ templates for background using events in data with $\not\!\!E_{\mathrm{T}} > 10\,\mathrm{GeV}$ and with the direction of the $\not\!\!E_{\mathrm{T}}$ vector along the photon-like jet. The estimated systematic uncertainty is obtained from the smallest bin in p_{T}^{γ} ($15 < p_{\mathrm{T}}^{\gamma} < 20\,\mathrm{GeV}$), as this is the bin that contains most of the background (Fig. 4) and corresponds to the largest control sample for input to the $\sigma_{\eta\eta}$ template representing the background. Based on the modified

templates, we assign a systematic uncertainty that reflects the largest discrepancy relative to the nominal yield, which is found to be 13% and 7% for the barrel and endcap, respectively. A more detailed discussion of systematic uncertainties in the background estimate is given in Section 5.4.

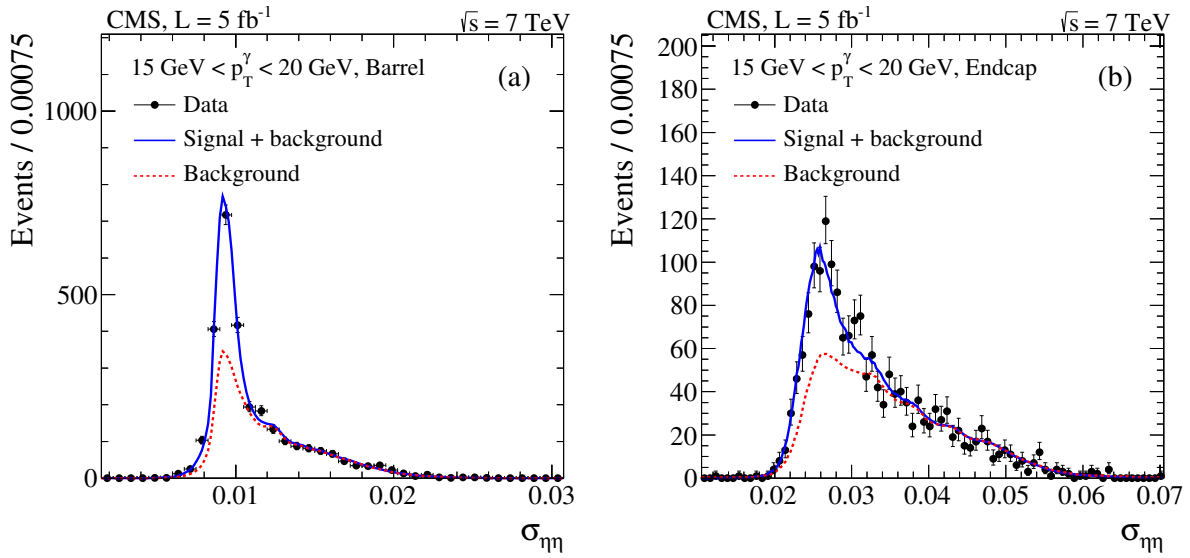

Figure 4: Fit to the $\sigma_{\eta\eta}$ distribution for photon candidates with $15 < p_{\mathrm{T}}^{\gamma} < 20\,\mathrm{GeV}$ in data with signal and background templates in the (a) barrel and (b) endcaps.

The systematic uncertainty in electron misidentification is estimated through changes made in the modeling of signal and background, the electron and photon energy resolutions, and the distributions for pileup in MC simulations.

The function fitted to the observed distribution of $\sigma_{\eta\eta}$ is the sum of contributions from signal (S) and background (B):

$$N_S S(\sigma_{\eta\eta}) + N_B B(\sigma_{\eta\eta}) = N\left[\frac{N_S}{N} S(\sigma_{\eta\eta}) + \left(1 - \frac{N_S}{N}\right) B(\sigma_{\eta\eta})\right], \tag{2}$$

where N, N_S, and N_B are the total number of events and the numbers of signal and background candidates in data for any given bin of p_{T}^{γ}, respectively. The $S(\sigma_{\eta\eta})$ and $B(\sigma_{\eta\eta})$ represent the expected signal and background distributions in $\sigma_{\eta\eta}$. These distributions are smoothed using a kernel-density estimator [30], or through direct interpolation when the statistical uncertainties are small, which makes it possible to use unbinned fits to the data in regions where statistics are poor, while preserving the good performance of the fit. The fit is calculated using an unbinned extended likelihood L and minimizes $-\ln L$ as a function of the signal fraction $f_S = N_S/N$:

$$-\ln L = (N_S + N_B) - \ln[f_S S(\sigma_{\eta\eta}) + (1 - f_S) B(\sigma_{\eta\eta})]. \tag{3}$$

4.1.2 Ratio method

We use a second method, referred to as the "ratio method," to infer the V+jets background as a cross-check of the results obtained with the template method at large p_{T}^{γ}, where the template method is subject to larger statistical uncertainties. The ratio method uses γ+jets and multijet data to extract the misidentification rate, taking into account the quark/gluon composition of the jets in V+jets events.

The ratio method exploits a category of jets that have properties similar to electromagnetic objects in the ECAL, and are called photon-like jets. Photon-like jets are jets selected through the presence of photons that pass all photon selection criteria, but fail either the photon isolation or $\sigma_{\eta\eta}$ requirements. However, these kinds of jets are still more isolated and have higher EM fractions than most generic jets.

The ratio method provides a ratio R_p of the probability for a jet to pass photon selection criteria to that of passing photon-like requirements. Once R_p is known, the number of jets that satisfy the final photon selection criteria ($N_{\mathrm{V+jets}}$) can be estimated as the product of R_p and the number of photon-like jets in data.

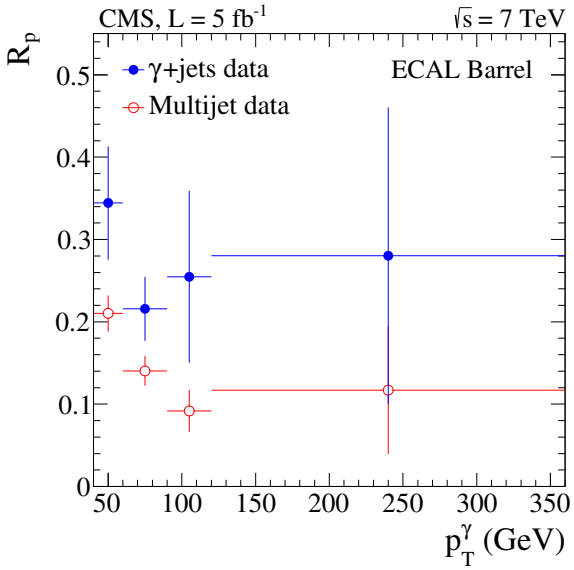

Figure 5: The R_p ratio (described in text) as a function of the p_{T} of photon candidates for the barrel region of the ECAL in γ+jets and multijet data. The difference in R_p values for the two processes is attributed to the fact that jets in γ+jets events are dominated by quark fragmentation, while jets in multijet events are dominated by gluon fragmentation.

We measure R_p separately for each p_{T}^{γ} bin of the analysis both for the barrel and endcap regions of the ECAL, using "diphoton" events, defined by the presence of either two photon candidates that pass the final photon selections, or that have one photon candidate that passes the final selections and one that passes only photon-like jet selections. To reduce correlations induced by the diphoton production kinematics, we require that the photons corresponding to each diphoton candidate be in the same η region and p_{T}^{γ} bin. A two-dimensional fit is performed based on templates of distributions in $\sigma_{\eta\eta}$ of each photon candidate to estimate R_p, and thereby subtract the contribution from genuine photons to the photon-like jet yield. As only 5–10% of genuine photons in multijet events pass photon-like jet requirements, we correct the distribution in R_p using MC simulation of multijet events, and check the correction through $\mathrm{Z} \to \mathrm{ee}$ data and simulation.

The observed R_p values for the barrel region of the ECAL are given in Fig. 5 as a function of p_{T}^{γ}. The difference between the two sets of R_p values extracted in different ways indicates the sensitivity of the method to whether the photon-like jet originates from hadronization of a quark or a gluon. We use the simulation of the gluon-to-quark jet ratio in W+jets and Z+jets events to correct R_p as a function of the p_{T} of the photon-like jet. We find the predictions from the ratio method to be consistent with those from the template method, and consider their

difference as an additional source of systematic uncertainty in the analysis.

4.2 Background from electrons misidentified as photons in $\ell\nu\gamma$ events

The criterion that differentiates electrons from photons is the presence in the pixel detector of a track that is associated with a shower in the ECAL. We use $Z \to ee$ data to measure the probability ($P_{e\to\gamma}$) for an electron not to have a matching track by requiring one of the electrons to pass stringent electron identification criteria, and then by checking how often the other electron passes the full photon selection criteria, including the requirement of having no associated track in the pixel detector. Fitting to the $m_{\ell\ell}$ distribution using a convolution of Breit–Wigner and "Crystal Ball" [31] functions to describe the signal and a falling exponential function for background, we obtain the probability for an electron to have no associated track as $P_{e\to\gamma} = 0.014 \pm 0.003\,(\text{syst.})$ and $0.028 \pm 0.004\,(\text{syst.})$ for the barrel and the endcap regions, respectively.

To estimate the background from sources where an electron is misidentified as a photon in the $\mu\nu\gamma$ channel, we select events that pass all event selection criteria except that the presence of a track in the pixel detector associated with the photon candidate is ignored. The contribution from genuine electrons misidentified as photons can therefore be calculated as

$$N_{e\to\gamma} = N_{\mu\nu e} \times \frac{P_{e\to\gamma}}{1 - P_{e\to\gamma}}, \tag{4}$$

where $N_{e\to\gamma}$ is the background from misidentified electrons and $N_{\mu\nu e}$ is the number of events selected without any requirement on the pixel track. The systematic uncertainties associated with this measurement are discussed in detail in Section 5.4.

The background in the $e\nu\gamma$ channel is dominated by Z+jets events, where one of the electrons from $Z \to ee$ decays is misidentified as a photon. To estimate the $Z \to ee$ contribution to the $W\gamma \to e\nu\gamma$ signal, we apply the full selection criteria and fit the invariant mass of the photon and electron candidates with a Breit–Wigner function convolved with a Crystal Ball function for the Z boson, and an exponential form for the background. Contributions to $e\nu\gamma$ events from other sources with genuine electrons misidentified as photons (e.g., $t\bar{t}$+jets and diboson processes) are estimated using MC simulation, in which a photon candidate is matched spatially to the generator-level electron.

4.3 Total background

The background from jets that are misidentified as photons is summarized as a function of p_T of the photon in Table 3 for $\ell\nu\gamma$ events and in Table 4 for $\ell\ell\gamma$ events, and the sums are listed as $N_B^{W+\text{jets}}$ in Table 5 and as $N_B^{Z+\text{jets}}$ in Table 6. The background from electrons in selected $\ell\nu\gamma$ events that are misidentified as photons, N_B^{eeX}, is summarized in Table 3 for both $e\nu\gamma$ and $\mu\nu\gamma$ channels. The N_B^{other} in Tables 5 and 6 indicates the rest of the background contributions estimated from simulation. For the $e\nu\gamma$ channel, the largest contribution to N_B^{other} (53%) is from $Z\gamma$ events, and the next largest is from γ+jets with a contribution of 33%. For the $\mu\nu\gamma$ channel, the dominant background to N_B^{other} is from $Z\gamma$, with a contribution of 84%. All the specific parameters will be discussed in more detail in Sections 5.4–5.6.

Table 3: Yield of misidentified photons from jets in W+jets events and their symmetrized associated systematic uncertainties as a function of p_{T}^{γ} in the $\mathrm{W}\gamma \to \ell\nu\gamma$ analyses. The results are specified in the second column by the numbers of events expected in the $\mathrm{e}\nu\gamma$ and $\mu\nu\gamma$ channels, and by the uncertainties from each of the sources in the rest of the columns.

		Systematic uncertainties on yields ($\mathrm{e}\nu\gamma/\mu\nu\gamma$)				
p_{T}^{γ} (GeV)	Yield from W+jets events	Shape of γ shower	Shape of jet shower	Sampling of distributions	Correlation of γ and $\not\!\!E_{\mathrm{T}}$	Diff. between jet $\to \gamma$ predictions
15–20	1450 / 2760	9.3 / 21	83 / 159	19 / 36	130 / 250	
20–25	650 / 1100	5.2 / 20	37 / 63	11 / 19	54 / 94	
25–30	365 / 520	3.7 / 9.4	21 / 30	9.4 / 14	33 / 43	
30–35	220 / 330	10.5 / 3.3	12 / 19	7.5 / 11	19 / 29	
35–40	160 / 200	3.4 / 2.8	10 / 12	6.2 / 7.9	14 / 16	
40–60	220 / 270	3.5 / 0.7	19 / 23	5.1 / 6.3	19 / 24	22 / 4.4
60–90	77 / 100	1.4 / 0.9	10 / 13	3.0 / 3.8	6.6 / 8.5	7.7 / 1.6
90–120	26 / 21	2.0 / 2.3	5.3 / 4.1	0.9 / 0.9	2.4 / 1.8	2.6 / 0.4
120–500	15 / 38	4.3 / 2.1	7.6 / 26	1.1 / 0.7	1.0 / 3.9	1.5 / 0.6
Totals	3180 / 5350	17 / 30	98 / 179	27 / 45	280 / 470	34 / 7.0
		300 / 510				

Table 4: Yield of misidentified photons from jets in Z+jets events and their symmetrized associated systematic uncertainties as a function of p_{T}^{γ} in the $\mathrm{Z}\gamma \to \ell\ell\gamma$ analyses. The results are specified by the numbers of events expected in the $\mathrm{ee}\gamma$ and $\mu\mu\gamma$ channels, and by the uncertainties from each of the sources.

		Systematic uncertainties on yields ($\mathrm{ee}\gamma/\mu\mu\gamma$)			
p_{T}^{γ} (GeV)	Yield from Z+jets events	Shape of γ shower	Shape of jet shower	Sampling of distributions	Diff. between jet $\to \gamma$ prediction
15–20	460 / 710	11 / 50	27 / 41	6.4 / 16	
20–25	200 / 310	6.8 / 23	11 / 18	3.7 / 6.7	
25–30	82 / 130	3.7 / 7.6	4.7 / 7.6	2.3 / 3.0	
30–35	51 / 82	2.8 / 10	2.9 / 4.7	1.9 / 1.8	
35–40	46 / 54	3.0 / 4.0	2.6 / 3.6	1.8 / 1.2	
40–60	40 / 72	3.8 / 11	2.3 / 5.8	0.9 / 1.5	11 / 9.5
60–90	18 / 25	3.0 / 6.5	1.1 / 3.6	0.7 / 0.6	4.8 / 3.2
90–120	0.0 / 14	0.0 / 3.8	0.0 / 1.9	0.0 / 0.3	0.0 / 4.4
120–500	5.3 / 6.6	4.6 / 13	0.4 / 1.4	0.1 / 0.2	1.4 / 3.6
Totals	910 / 1400	16 / 59	30 / 46	8.3 / 18	17 / 12
		38 / 77			

Table 5: Summary of parameters used in the measurement of the $\mathrm{W}\gamma$ cross section.

Parameter	$\mathrm{e}\nu\gamma$ channel	$\mu\nu\gamma$ channel
$N^{\ell\nu\gamma}$	7470	10 809
$N_B^{\mathrm{W+jets}}$	$3180 \pm 50\,(\mathrm{stat.}) \pm 300\,(\mathrm{syst.})$	$5350 \pm 60\,(\mathrm{stat.}) \pm 510\,(\mathrm{syst.})$
N_B^{eeX}	$690 \pm 20\,(\mathrm{stat.}) \pm 50\,(\mathrm{syst.})$	$91 \pm 1\,(\mathrm{stat.}) \pm 5\,(\mathrm{syst.})$
N_B^{other}	$410 \pm 20\,(\mathrm{stat.}) \pm 30\,(\mathrm{syst.})$	$400 \pm 20\,(\mathrm{stat.}) \pm 30\,(\mathrm{syst.})$
$N_S^{\ell\nu\gamma}$	$3200 \pm 100\,(\mathrm{stat.}) \pm 320\,(\mathrm{syst.})$	$4970 \pm 120\,(\mathrm{stat.}) \pm 530\,(\mathrm{syst.})$
A_S	$0.108 \pm 0.001\,(\mathrm{stat.})$	$0.087 \pm 0.001\,(\mathrm{stat.})$
$A_S \cdot \epsilon_{\mathrm{MC}}$ ($\mathrm{W}\gamma \to \ell\nu\gamma$)	$0.0187 \pm 0.0010\,(\mathrm{syst.})$	$0.0270 \pm 0.0014\,(\mathrm{syst.})$
ρ_{eff}	$0.940 \pm 0.027\,(\mathrm{syst.})$	$0.990 \pm 0.025\,(\mathrm{syst.})$
L (fb^{-1})	$5.0 \pm 0.1\,(\mathrm{syst.})$	$5.0 \pm 0.1\,(\mathrm{syst.})$

Table 6: Summary of parameters used in the measurement of the $Z\gamma$ cross section.

Parameter	eeγ channel	$\mu\mu\gamma$ channel
$N^{\ell\ell\gamma}$	4108	6463
$N_B^{\text{Z+jets}}$	$910 \pm 50\,(\text{stat.}) \pm 40\,(\text{syst.})$	$1400 \pm 60\,(\text{stat.}) \pm 80\,(\text{syst.})$
N_B^{other}	$40 \pm 3\,(\text{stat.})$	$24 \pm 2\,(\text{stat.})$
$N_S^{\ell\ell\gamma}$	$3160 \pm 80\,(\text{stat.}) \pm 90\,(\text{syst.})$	$5030 \pm 100\,(\text{stat.}) \pm 210\,(\text{syst.})$
A_S	$0.249 \pm 0.001\,(\text{stat.})$	$0.286 \pm 0.001\,(\text{stat.})$
$A_S \cdot \epsilon_{\text{MC}}$ ($Z\gamma \to \ell\ell\gamma$)	$0.1319 \pm 0.0018\,(\text{syst.})$	$0.1963 \pm 0.0013\,(\text{stat.})$
ρ_{eff}	$0.929 \pm 0.047\,(\text{syst.})$	$0.945 \pm 0.016\,(\text{syst.})$
L (fb^{-1})	$5.0 \pm 0.1\,(\text{syst.})$	$5.0 \pm 0.1\,(\text{syst.})$

5 Results

5.1 The Wγ process and radiation-amplitude zero

For photon transverse momenta >15 GeV and angular separations between the charged leptons and photons of $\Delta R > 0.7$, the Wγ production cross section at NLO for each leptonic decay channel is expected to be 31.8 ± 1.8 pb [19, 20]. This cross section point is used to normalize the p_{T}^{γ} distributions for the signal in Fig. 6, which shows good agreement of the data with the expectations from the SM.

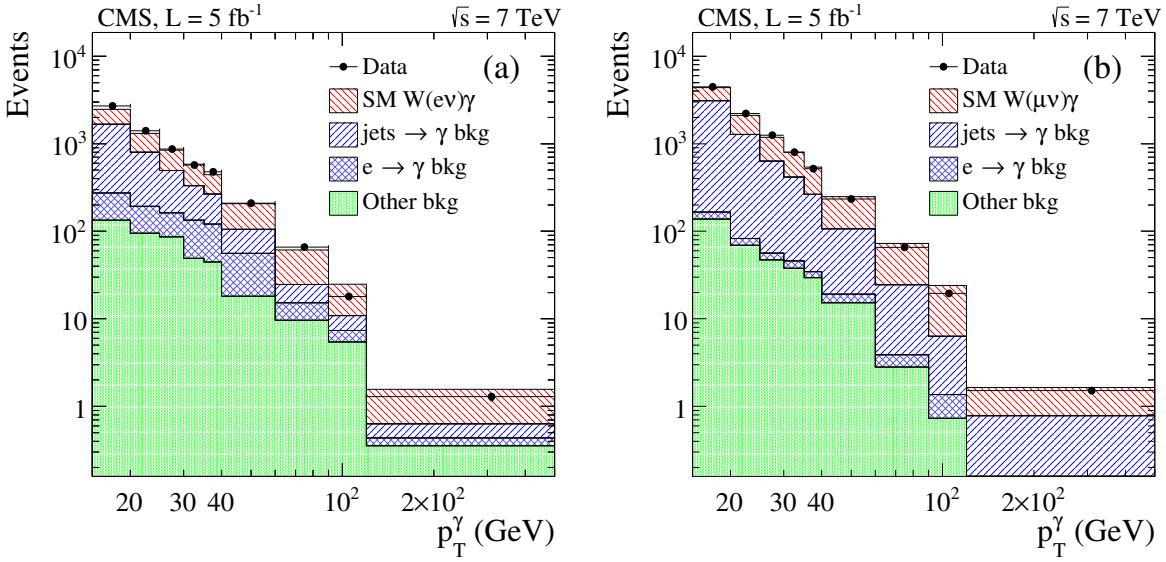

Figure 6: Distributions in p_{T}^{γ} for Wγ candidate events in data, with signal and background MC simulation contributions to (a) W$\gamma \to e\nu\gamma$ and (b) W$\gamma \to \mu\nu\gamma$ channels shown for comparison.

The three leading-order Wγ production diagrams in Fig. 1 interfere with each other, resulting in a vanishing of the yield at specific regions of phase space. Such phenomena are referred to as radiation-amplitude zeros (RAZ) [32–36], and the effect was first observed by the D0 Collaboration [6] using the charge-signed rapidity difference $Q_\ell \times \Delta\eta$ between the photon candidate and the charged lepton candidate from $W \to \ell\nu$ decays [37]. In the SM, the minimum is at $Q_\ell \times \Delta\eta = 0$ for pp collisions. Anomalous Wγ contributions can affect the distribution in $Q_\ell \times \Delta\eta$ and make the minimum less pronounced. The differential yield as a function of charge-signed rapidity difference, shown in Fig. 7(a) for Wγ events normalized to the yield of signal in data, is obtained with the additional requirements of having no accompanying jets

with $p_T > 30$ GeV and a transverse three-body mass, or cluster mass [37], of the photon, lepton, and $\not\!\!E_T$ system > 110 GeV. The three body mass $M_T(\ell\gamma\not\!\!E_T)$ is calculated as

$$M_T(\ell\gamma\not\!\!E_T)^2 = \left[(M^2_{\ell\gamma} + |\mathbf{p}_T(\gamma) + \mathbf{p}_T(\ell)|^2)^{1/2} + \not\!\!E_T\right]^2 - |\mathbf{p}_T(\gamma) + \mathbf{p}_T(\ell) + \not\!\!\mathbf{E}_T|^2, \quad (5)$$

where $M_{\ell\gamma}$ denotes the invariant mass of the $\ell\gamma$ system, and $\mathbf{p}_T(i)$, $i = \gamma$, ℓ, and $\not\!\!E_T$ are the projections of the photon, lepton, and $\not\!\!E_T$ vectors on the transverse plane, respectively. Figure 7(b) shows the background-subtracted data. The shaded bars indicate statistical and systematic uncertainties on the MC prediction. The distributions demonstrate the characteristic RAZ expected for Wγ production. Both figures indicate no significant difference between data and expectations from SM MC simulations.

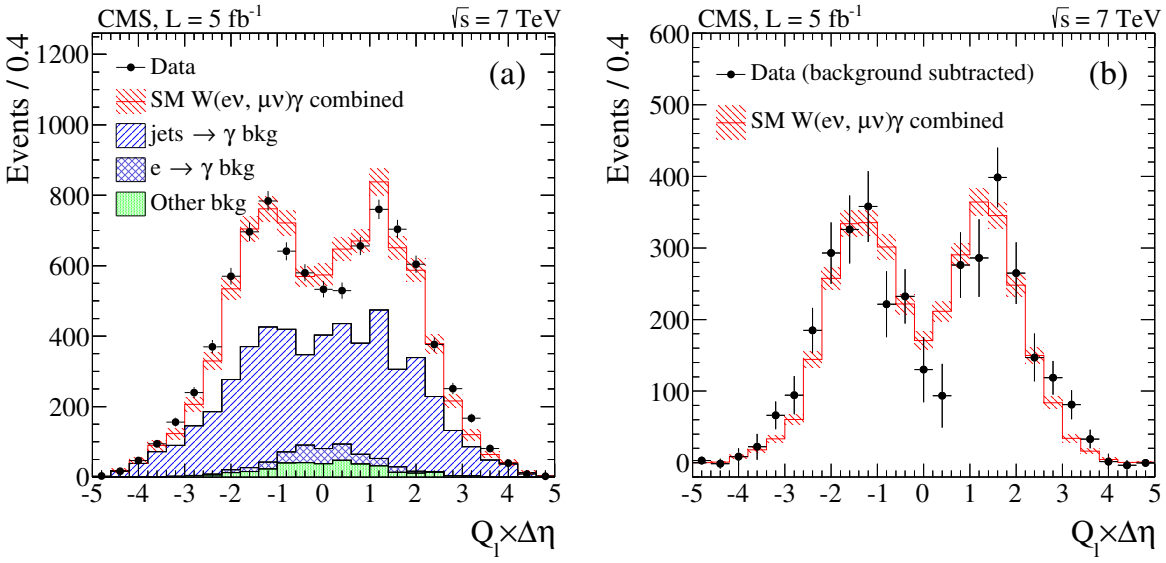

Figure 7: Charge-signed rapidity difference $Q_\ell \times \Delta\eta$ between the photon candidate and a lepton for Wγ candidates in data (filled circles) and expected SM signal and backgrounds (shaded regions) normalized to (a) data, and (b) background-subtracted data. The hatched bands illustrate the full uncertainty in the MC prediction.

5.2 The $Z\gamma$ process

The cross section for $Z\gamma$ production at NLO in the SM, for $p_T^\gamma > 15$ GeV, $\Delta R(\ell, \gamma) > 0.7$ between the photon and either of the charged leptons from the $Z \to \ell^+\ell^-$ decay, and $m_{\ell\ell} > 50$ GeV, is predicted to be 5.45 ± 0.27 pb [19, 20]. After applying all selection criteria, the p_T^γ distributions for data and contributions expected from MC simulation are shown for eeγ and $\mu\mu\gamma$ final states in Figs. 8(a) and (b), respectively. Again, good agreement is found between data and the SM predictions.

5.3 Production cross sections

The cross section for any signal process of interest can be written as

$$\sigma_S = \frac{N_S}{A_S \cdot \epsilon_S \cdot \mathrm{L}}\ , \quad (6)$$

where N_S is the number of observed signal events, A_S is the geometric and kinematic acceptance of the detector, ϵ_S is the selection efficiency for signal events in the region of acceptance,

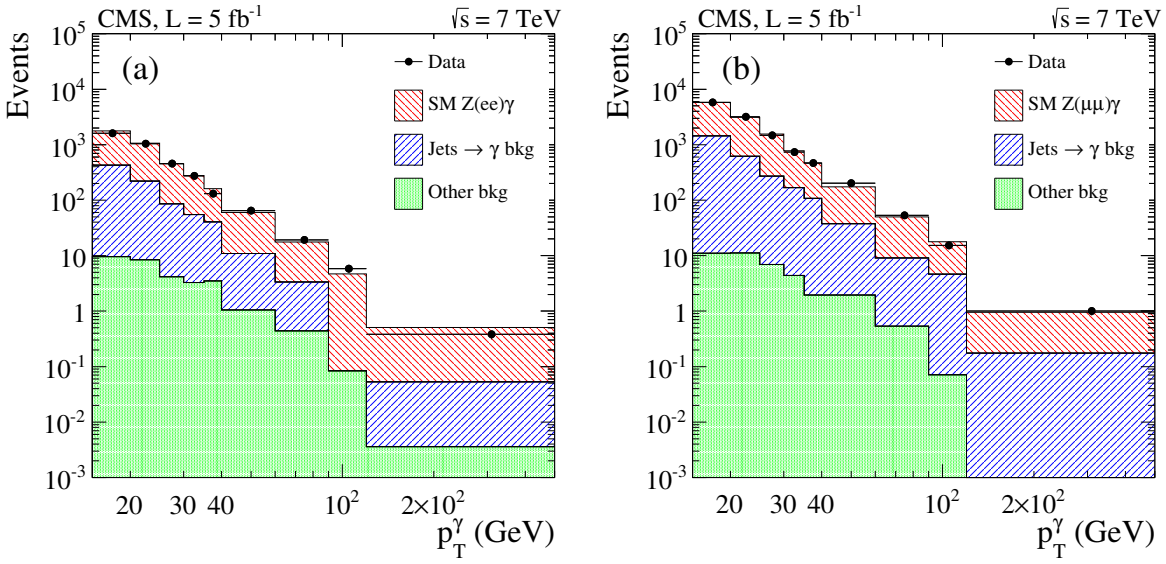

Figure 8: Distributions in p_{T}^{γ} for $\mathrm{Z}\gamma$ candidate events in data, with signal and background MC simulation contributions to (a) $\mathrm{Z}\gamma \to \mathrm{ee}\gamma$ and (b) $\mathrm{Z}\gamma \to \mu\mu\gamma$ channels shown for comparison.

and L is the integrated luminosity. The value of A_S in our analyses is calculated through MC simulation, and is affected by the choice of PDF and other uncertainties of the model, while the value of ϵ_S is sensitive to uncertainties in the simulation, triggering, and reconstruction. To reduce uncertainties in efficiency, we apply corrections to the efficiencies obtained from MC simulation, which reflect ratios of efficiencies $\rho_{\mathrm{eff}} = \epsilon_{\mathrm{data}}/\epsilon_{\mathrm{MC}}$ obtained by measuring the efficiency in the same way for data and simulation. The product $A_S \times \epsilon_S$ can then be replaced by the product $\mathcal{F}_S \times \rho_{\mathrm{eff}}$, where $\mathcal{F}_S \equiv A_S \times \epsilon_{\mathrm{MC}}$ corresponds to the fraction of generated signal events selected in the simulation.

Equation (6) can therefore be rewritten as

$$\sigma_S = \frac{N - N_B}{\mathcal{F}_S \cdot \rho_{\mathrm{eff}} \cdot \mathrm{L}}, \tag{7}$$

in which we replace the number of signal events N_S by subtracting the estimated number of background events N_B from the observed number of selected events N.

We calculate $\mathcal{F}_S$ using MC simulation, with $\mathcal{F}_S$ defined by $N_{\mathrm{accept}}/N_{\mathrm{gen}}$, where N_{accept} is the number of signal events that pass all selection requirements in the MC simulation of signal, and N_{gen} is the number of MC generated events restricted to $p_{\mathrm{T}}^{\gamma} > 15\,\mathrm{GeV}$ and $\Delta R(\ell, \gamma) > 0.7$, for $\mathrm{W}\gamma$, and with an additional requirement, $m_{\ell\ell} > 50\,\mathrm{GeV}$, for $\mathrm{Z}\gamma$.

5.4 Systematic uncertainties

Systematic uncertainties are grouped into five categories. The first group includes uncertainties that affect the signal, such as uncertainties on lepton and photon energy scales. We change the electron energy scale in data by its estimated uncertainty of 0.5% in barrel and 3% in endcaps, to gauge the contribution from the calibration of the ECAL detector. For the muon channel, the muon momentum is changed by 0.2%. For photons, we change the energy by 1% and 3% in the EB and EE region, respectively. The systematic effect on the measured cross section is obtained by reevaluating N_S for such changes in each source of systematic uncertainty. To extract the systematic effect of the energy scale on the signal yield, the data-driven background estimation

is performed using signal and background templates modified to use the varied energy scale. This ensures that migrations of photons and misidentified photon-like jets across the low-p_{T}^{γ} boundaries are properly taken into account for this systematic uncertainty.

In the second group, we combine uncertainties that affect the product of the acceptance, reconstruction, and identification efficiencies of final state objects, as determined from simulation. These include uncertainties in the lepton and photon energy resolution, effects from pileup, and uncertainties in the PDF. The uncertainty in the product of acceptance and efficiency ($A_S \times \epsilon_S$) is determined from MC simulation of the Vγ signal and is affected by the lepton and photon energy resolution through the migration of events in and out of the acceptance. The electron energy resolution is determined from data using the observed width of the Z boson peak in the $\mathrm{Z} \to \mathrm{ee}$ events, following the same procedure as employed in Ref. [38]. To estimate the effect of electron resolution on $A_S \times \epsilon_S$, each electron candidate's energy is smeared randomly by the energy resolution determined from data, before applying the standard selections. The photon energy resolution is determined simultaneously with the photon energy scale from data, following the description in Ref. [28]. The systematic effect of photon resolution on $A_S \times \epsilon_S$ is calculated by smearing the reconstructed photon energy in simulation to match that in data.

The number of pileup interactions per event is estimated from data using a convolution procedure that extracts the estimated pileup from the instantaneous bunch luminosity. The total inelastic pp scattering cross section is used to estimate the number of pileup interactions expected in a given bunch crossing, with a systematic uncertainty from modeling of the pileup interactions obtained by changing the total inelastic cross section within its uncertainties [39] to determine the impact on $A_S \times \epsilon_S$. The uncertainties from the choice of PDF are estimated using the CTEQ6.6 PDF set [21]. The uncertainty in the modeling of the signal is taken from the difference in acceptance between MCFM and MADGRAPH predictions.

The third group of uncertainties includes the systematic sources affecting the relative ρ_{eff} correction factors for efficiencies of the trigger, reconstruction, and identification requirements in simulations and data. Among these sources are the uncertainties in lepton triggers, lepton and photon reconstruction and identification, and $\not\!\!E_{\mathrm{T}}$ for the Wγ process. The uncertainties in lepton and photon efficiencies are estimated by changing the modeling of background and the range of the fits used in the tag-and-probe method.

The fourth category of uncertainties comprises the contributions from background. These are dominated by uncertainties in estimating the W+jets and Z+jets backgrounds from data. The difference in $\sigma_{\eta\eta}$ distributions between data and simulated events (Section 4.1.1) is attributed to systematic uncertainties in signal templates, which are used to calculate the background estimate and measure its effect on the final result. To infer the background from photon-like jets that pass full photon-isolation criteria, we use the $\sigma_{\eta\eta}$ distributions obtained by reversing the original isolation requirement for the tracker. The possible correlation of $\sigma_{\eta\eta}$ with tracker isolation, and a contribution from genuine photons that pass the reversed isolation requirement, can cause bias in the estimation of background. The first issue is investigated by comparing the sideband and true $\sigma_{\eta\eta}$ distributions in simulated multijets events, where genuine photons can be distinguished from jets. The resulting bias on the background estimation is shown by the open circles in Fig. 9. The second issue, concerning the contamination of the background template by signal, is investigated by comparing the sideband $\sigma_{\eta\eta}$ distributions of simulated samples, both with and without admixtures of genuine photons. The results of the bias studies are shown by the open squares in Fig. 9, and the overall effect, given by the filled black circles, is found to be small.

Since smoothing is used to define a continuous function for describing the $\sigma_{\eta\eta}$ distribution for

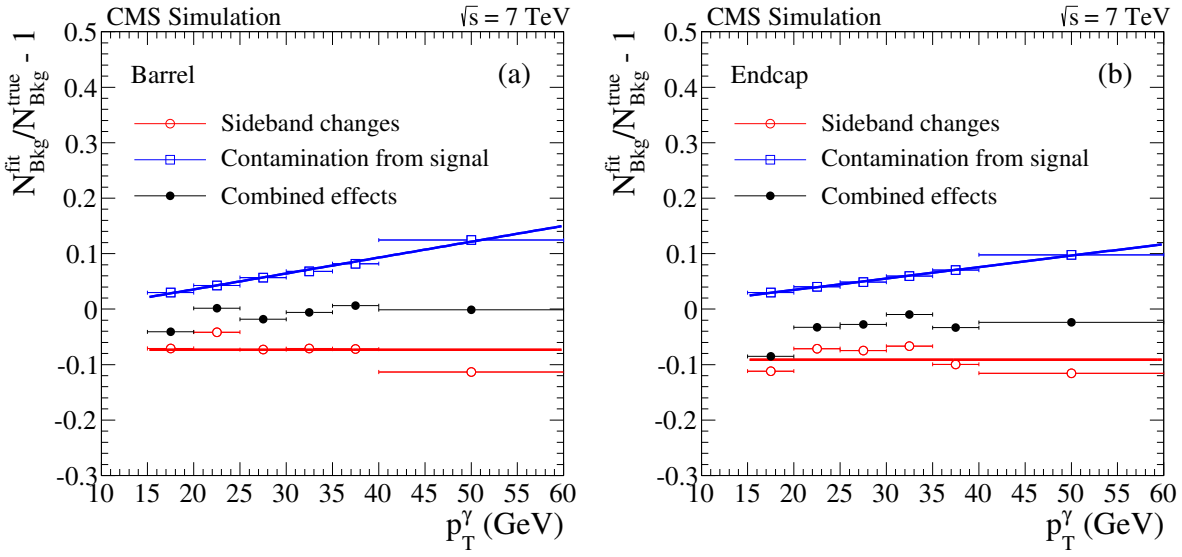

Figure 9: Bias in the background contamination related to the background templates for $\sigma_{\eta\eta}$, as a function of p_T^{γ}, for the (a) barrel and (b) endcap regions of ECAL.

background, the effect of statistical sampling of the background probability density requires an appreciation of the features of the underlying distribution. This is studied as follows. The simulation is used to generate a distribution for background, which can be used to generate a template. These new distributions are also smoothed, and used to fit the background fraction in data. The results of fits using each such distribution are saved, and the standard deviation associated with the statistical fluctuation in the template is taken as a systematic uncertainty. The systematic uncertainties from different inputs in the estimation of background from W+jets and Z+jets events were shown in Table 3 and 4, respectively.

The uncertainties in background from electrons misidentified as photons in Wγ candidate events are estimated by taking the difference in $P_{e\to\gamma}$ between the measurement described in Section 4.2 and that obtained using a simple counting method. The uncertainties for lesser contributions to background are defined by the statistical uncertainties in the samples used for their simulation. Finally, the systematic uncertainty in the measured integrated luminosity is 2.2% [40].

5.5 Wγ cross section

In the summary of parameters used in the measurement of the pp $\to$ Wγ cross sections listed in Table 5, $N^{\ell\nu\gamma}$ is the number of observed events, $N_S^{\ell\nu\gamma}$ is the number of observed signal events after background subtraction, and $A_S \times \epsilon_S$, ρ_{eff}, and L are described in Section 5.3. A summary of all systematic uncertainties in the measured Wγ cross sections is given in Table 7, separately for electron and muon channels.

The measured cross sections are

$$\sigma(\text{pp} \to \text{W}\gamma) \times \mathcal{B}(\text{W} \to \text{e}\nu) = 36.6 \pm 1.2\,(\text{stat.}) \pm 4.3\,(\text{syst.}) \pm 0.8\,(\text{lum.})\,\text{pb},$$

$$\sigma(\text{pp} \to \text{W}\gamma) \times \mathcal{B}(\text{W} \to \mu\nu) = 37.5 \pm 0.9\,(\text{stat.}) \pm 4.5\,(\text{syst.}) \pm 0.8\,(\text{lum.})\,\text{pb}.$$

The mean of these cross sections, obtained using a best linear unbiased estimator (BLUE) [41], is

$$\sigma(\text{pp} \to \text{W}\gamma) \times \mathcal{B}(\text{W} \to \ell\nu) = 37.0 \pm 0.8\,(\text{stat.}) \pm 4.0\,(\text{syst.}) \pm 0.8\,(\text{lum.})\,\text{pb}.$$

Table 7: Summary of systematic uncertainties in the measurement of Wγ cross section, separated into the main groups of sources for the e$\nu\gamma$ and $\mu\nu\gamma$ channels. "n/a" stands for "not applicable".

		e$\nu\gamma$	$\mu\nu\gamma$
Source (Group 1)	Uncertainties	Effect from N_{sig}	
e/γ energy scale	(e: 0.5%; γ: 1% (EB), 3% (EE))	2.9%	n/a
γ energy scale	(1% (EB), 3% (EE))	n/a	2.9%
μ p_{T} scale	(0.2%)	n/a	0.6%
Total uncertainty in N_{sig}		2.9%	3.0%
Source (Group 2)	Uncertainties	Effect from $\mathcal{F}_S = A_S \cdot \epsilon_S$	
e/γ energy resolution	(1% (EB), 3% (EE))	0.3%	n/a
γ energy resolution	(1% (EB), 3% (EE))	n/a	0.1%
μ p_{T} resolution	(0.6%)	n/a	0.1%
Pileup	(Shift pileup distribution by $\pm$ 5%)	2.4%	0.8%
PDF		0.9%	0.9%
Modeling of signal		5.0%	5.0%
Total uncertainty in $\mathcal{F}_S = A_S \cdot \epsilon_S$		5.6%	5.1%
Source (Group 3)	Uncertainties	Effect from ρ_{eff}	
Lepton reconstruction		0.4%	1.5%
Lepton trigger		0.1%	0.9%
Lepton ID and isolation		2.5%	0.9%
$\not{E}_{\text{T}}$ selection		1.4%	1.5%
γ identification and isolation	(0.5% (EB), 1.0% (EE))	0.5%	0.5%
Total uncertainty in ρ_{eff}		2.9%	2.5%
Source (Group 4)		Effect from background yield	
Template method		9.3%	10.2%
Electron misidentification		1.5%	0.1%
MC prediction		0.8%	0.5%
Total uncertainty due to background		9.5%	10.2%
Source (Group 5)			
Luminosity		2.2%	2.2%

All three results are consistent within uncertainties with the NLO prediction of 31.8 ± 1.8 pb, computed with MCFM. The uncertainty on the prediction is obtained using the CTEQ6.6 PDF set [21].

5.6 $Z\gamma$ cross section

In the summary of parameters used in the measurement of the pp $\to$ Zγ cross section listed in Table 6, $N^{\ell\ell\gamma}$ is the number of observed events, and $N_S^{\ell\ell\gamma}$ is the number of observed signal events after background subtraction. The systematic uncertainties for the measurement of the $Z\gamma$ cross sections are listed in Table 8. The cross sections for the two channels are

$$\sigma(\text{pp} \to \text{Z}\gamma) \times \mathcal{B}(\text{Z} \to \text{ee}) = 5.20 \pm 0.13\,(\text{stat.}) \pm 0.32\,(\text{syst.}) \pm 0.11\,(\text{lum.})\,\text{pb},$$

$$\sigma(\text{pp} \to \text{Z}\gamma) \times \mathcal{B}(\text{Z} \to \mu\mu) = 5.43 \pm 0.10\,(\text{stat.}) \pm 0.29\,(\text{syst.}) \pm 0.12\,(\text{lum.})\,\text{pb},$$

and their mean, extracted using the BLUE method is

$$\sigma(\text{pp} \to \text{Z}\gamma) \times \mathcal{B}(\text{Z} \to \ell\ell) = 5.33 \pm 0.08\,(\text{stat.}) \pm 0.25\,(\text{syst.}) \pm 0.12\,(\text{lum.})\,\text{pb}.$$

All three results are also consistent within the uncertainties with the theoretical NLO cross section of 5.45 ± 0.27 pb, computed with MCFM. The uncertainty on the prediction is obtained using the CTEQ6.6 PDF set [21].

Table 8: Summary of systematic uncertainties for the measurement of the Zγ cross section. "n/a" stands for "not applicable".

		eeγ	$\mu\mu\gamma$
Source (Group 1)	Uncertainties	Effect from N_{sig}	
e energy scale	(0.5%)	3.0%	n/a
μ p_{T} scale	(0.2%)	n/a	0.6%
γ energy scale	(1% (EB), 3% (EE))	n/a	4.2%
Total uncertainty in N_{sig}		3.0%	4.2%
Source (Group 2)	Uncertainties	Effect from $\mathcal{F}_S = A_S \cdot \epsilon_S$	
e/γ energy resolution	(1% (EB), 3% (EE))	0.2%	n/a
γ energy resolution	(1% (EB), 3% (EE))	n/a	0.1%
μ p_{T} resolution	(0.6%)	n/a	0.2%
Pileup	Shift pileup distribution by $\pm$ 5%	0.6%	0.4%
PDF		1.1%	1.1%
Modeling of signal		0.6%	0.5%
Total uncertainty in $\mathcal{F}_S = A_S \cdot \epsilon_S$		1.4%	1.3%
Source (Group 3)	Uncertainties	Effect from ρ_{eff}	
Lepton reconstruction		0.8%	1.0%
Lepton trigger		0.1%	1.0%
Lepton ID and isolation		5.0%	1.8%
Photon ID and isolation	(0.5% (EB), 1.0% (EE))	0.5%	1.0%
Total uncertainty in ρ_{eff}		5.1%	2.5%
Source (Group 4)		Effect from background yield	
Template method		1.2%	1.5%
Total uncertainty due to background		1.2%	1.5%
Source (Group 5)			
Luminosity		2.2%	2.2%

5.7 Ratio of Wγ and Zγ production cross sections

We calculate the ratio of the Wγ and Zγ cross sections using the BLUE method to account for correlated systematic uncertainties between individual channels for both measurements and predictions. The MCFM prediction of 5.8 ± 0.1 is consistent with the measured ratio, $6.9 \pm 0.2\,(\text{stat.}) \pm 0.5\,(\text{syst.})$.

5.8 Comparisons to MCFM predictions

Finally, we present a summary of the Wγ and Zγ cross sections measured with larger requirements on the minimum photon p_{T}^{γ}. After accounting for all systematic uncertainties for $p_{\text{T}}^{\gamma} > 60$ and >90 GeV, we find no significant disagreement with the MCFM predictions for Vγ processes. These cross sections, predictions, and their uncertainties are summarized in Table 9 and in Fig. 10.

Table 9: Summary of the measured cross sections and predictions for $p_T^\gamma > 60$ and > 90 GeV for Wγ and Zγ production.

Process	p_T^γ (GeV)	$\sigma \times \mathcal{B}$ (pb)	Theory (pb)
$W\gamma \to e\nu\gamma$	> 60	0.77 ± 0.07 (stat.) ± 0.13 (syst.) ± 0.02 (lum.)	0.58 ± 0.08
$W\gamma \to \mu\nu\gamma$	> 60	0.76 ± 0.06 (stat.) ± 0.08 (syst.) ± 0.02 (lum.)	0.58 ± 0.08
$W\gamma \to \ell\nu\gamma$	> 60	0.76 ± 0.05 (stat.) ± 0.08 (syst.) ± 0.02 (lum.)	0.58 ± 0.08
$W\gamma \to e\nu\gamma$	> 90	0.17 ± 0.03 (stat.) ± 0.04 (syst.) ± 0.01 (lum.)	0.17 ± 0.03
$W\gamma \to \mu\nu\gamma$	> 90	0.25 ± 0.04 (stat.) ± 0.05 (syst.) ± 0.01 (lum.)	0.17 ± 0.03
$W\gamma \to \ell\nu\gamma$	> 90	0.20 ± 0.03 (stat.) ± 0.04 (syst.) ± 0.01 (lum.)	0.17 ± 0.03
$Z\gamma \to ee\gamma$	> 60	0.14 ± 0.02 (stat.) ± 0.02 (syst.) ± 0.01 (lum.)	0.12 ± 0.01
$Z\gamma \to \mu\mu\gamma$	> 60	0.14 ± 0.01 (stat.) ± 0.02 (syst.) ± 0.01 (lum.)	0.12 ± 0.01
$Z\gamma \to \ell\ell\gamma$	> 60	0.14 ± 0.01 (stat.) ± 0.01 (syst.) ± 0.01 (lum.)	0.12 ± 0.01
$Z\gamma \to ee\gamma$	> 90	0.047 ± 0.013 (stat.) ± 0.010 (syst.) ± 0.001 (lum.)	0.040 ± 0.004
$Z\gamma \to \mu\mu\gamma$	> 90	0.046 ± 0.008 (stat.) ± 0.010 (syst.) ± 0.001 (lum.)	0.040 ± 0.004
$Z\gamma \to \ell\ell\gamma$	> 90	0.046 ± 0.007 (stat.) ± 0.009 (syst.) ± 0.001 (lum.)	0.040 ± 0.004

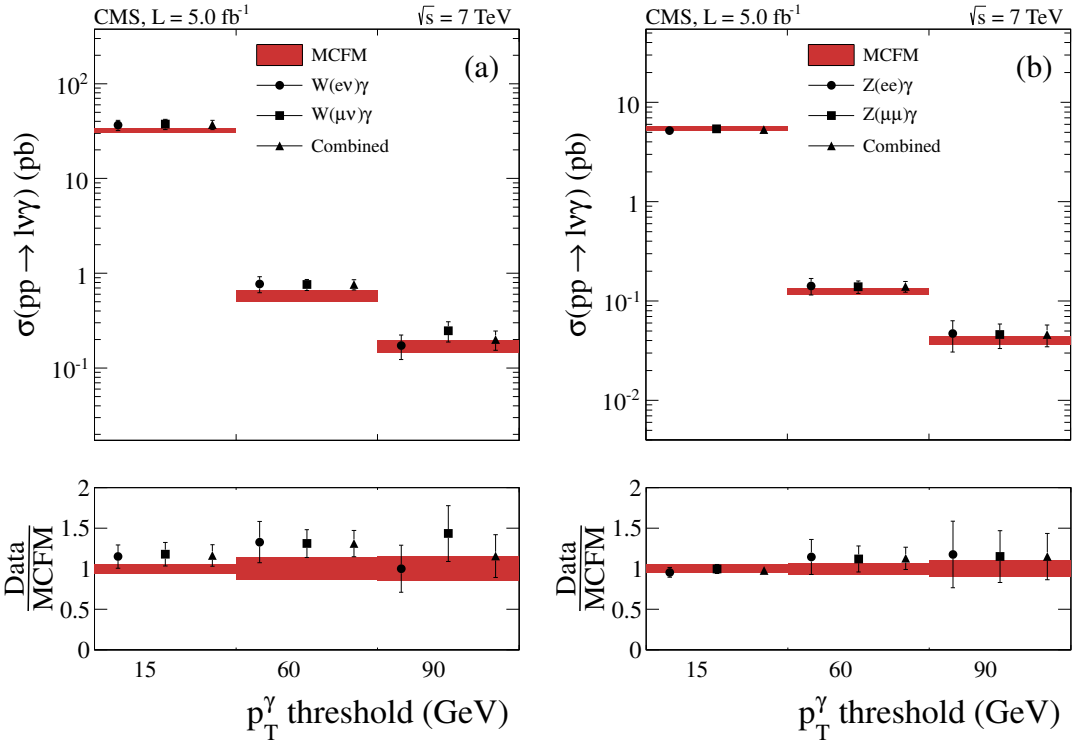

Figure 10: A summary of measured cross sections for three p_T^γ thresholds, compared to SM predictions for (a) Wγ and (b) Zγ production.

6 Anomalous triple gauge couplings in Wγ and Zγ production

6.1 WWγ coupling

The most general Lorentz invariant, effective Lagrangian that describes WWγ and WWZ couplings has 14 independent parameters [42, 43], seven for each triple-boson vertex. Assuming charge conjugation (C) and parity (P) invariance for the effective EW Lagrangian ($\mathcal{L}_{WWV}$), normalized by its EW coupling strength (g_{WWV}), leaves only six independent couplings for de-

scribing the WWγ and WWZ vertices:

$$\frac{\mathcal{L}_{\mathrm{WWV}}}{g_{\mathrm{WWV}}} = ig_1^V(W^\dagger_{\mu\nu}W^\mu V^\nu - W^\dagger_\mu V_\nu W^{\mu\nu}) + i\kappa_V W^\dagger_\mu W_\nu V^{\mu\nu} + \frac{i\lambda_V}{M_W^2} W^\dagger_{\delta\mu} W^\mu_\nu V^{\nu\delta}, \tag{8}$$

where V $=\gamma$ or Z, W^μ are the $W^\pm$ fields, $W_{\mu\nu} = \partial_\mu W_\nu - \partial_\nu W_\mu$, with the overall couplings given by $g_{\mathrm{WW}\gamma} = -e$, and $g_{\mathrm{WWZ}} = -e\cot\theta_W$, where θ_W is the weak mixing angle. Assuming electromagnetic gauge invariance, $g_1^\gamma = 1$; the remaining parameters that describe the WWγ and WWZ couplings are g_1^Z, κ_Z, κ_γ, λ_Z, and λ_γ. In the SM, $\lambda_\mathrm{Z} = \lambda_\gamma = 0$ and $g_1^\mathrm{Z} = \kappa_\mathrm{Z} = \kappa_\gamma = 1$. In this analysis, we follow the convention that describes the couplings in terms of their deviation from the SM values: $\Delta g_1^\mathrm{Z} \equiv g_1^\mathrm{Z} - 1$, $\Delta\kappa_\mathrm{Z} \equiv \kappa_\mathrm{Z} - 1$, and $\Delta\kappa_\gamma \equiv \kappa_\gamma - 1$. Invariance under $SU(2)_L \times U(1)_Y$ transformations reduces these to three independent couplings:

$$\Delta\kappa_\mathrm{Z} = \Delta g_1^\mathrm{Z} - \Delta\kappa_\gamma \cdot \tan^2\theta_\mathrm{W}, \quad \lambda = \lambda_\gamma = \lambda_\mathrm{Z}, \tag{9}$$

where $\Delta\kappa_\gamma$ and λ_γ are determined from Wγ production.

6.2 ZZγ and Z$\gamma\gamma$ couplings

The most general vertex function for ZZγ [44] can be written as

$$\begin{aligned}\Gamma^{\alpha\beta\mu}_{\mathrm{ZZ}\gamma}(q_1,q_2,p) = \frac{p^2-q_1^2}{m_\mathrm{Z}^2}\Bigg[& h_1^\mathrm{Z}(q_2^\mu g^{\alpha\beta} - q_2^\alpha g^{\mu\beta}) \\ & + \frac{h_2^\mathrm{Z}}{m_\mathrm{Z}^2} p^\alpha \left[(p\cdot q_2)g^{\mu\beta} - g_2^\mu p^\beta\right] \\ & + h_3^\mathrm{Z}\epsilon^{\mu\alpha\beta\rho}q_{2\rho} \\ & + \frac{h_4^\mathrm{Z}}{m_\mathrm{Z}^2} p^\alpha \epsilon^{\mu\beta\rho\sigma} p_\rho q_{2\sigma}\Bigg],\end{aligned} \tag{10}$$

with the Z$\gamma\gamma$ vertex obtained by the replacements

$$\frac{p^2-q_1^2}{m_\mathrm{Z}^2} \to \frac{p^2}{m_\mathrm{Z}^2} \text{ and } h_i^\mathrm{Z} \to h_i^\gamma,\ i = 1,\ldots,4. \tag{11}$$

The couplings h_i^V for V = Z or γ, and $i = 1,2$, violate CP symmetry, while those with $i = 3,4$ are CP-even. Although, at tree level, all these couplings vanish in the SM, at the higher, one-loop level, the CP-conserving couplings are $\approx 10^{-4}$. As the sensitivity to CP-odd and CP-even couplings is the same when using p_T^γ to check for the presence of contributions from ATGCs, we interpret the results as limits on h_3^V and h_4^V only.

6.3 Search for anomalous couplings in Wγ and Zγ production

To extract limits on the ATGCs, we simply count the yield of events in bins of p_T^γ. The 95% confidence level (CL) upper limits on values of ATGCs are set using the modified frequentist CL_s method [45].

As the simulation of the ATGC signal is not available in MADGRAPH, the signals are generated using the SHERPA MC program [18] to simulate Wγ+jets and Zγ+jets with up to two jets in the final state.

For the Wγ analysis, we set one and two-dimensional limits on each ATGC parameter $\Delta\kappa_\gamma$ and λ_γ, while g_1^Z is set to the SM value, assuming the "equal couplings" scenario of the LEP parameterization [46].

For the Zγ analysis, we set h_1^V and h_2^V to the SM values, and set two-dimensional limits on the h_3^V and h_4^V anomalous couplings, with V = Z or γ. For limits set on the Z-type couplings, the γ couplings are set to their SM values, i.e., to zero, and vice versa. In this study, we follow the CMS convention of not suppressing the anomalous TGCs by an energy-dependent form factor.

The two-dimensional contours for upper limits at the 95% confidence level are given in Fig. 11 for the Wγ, and Fig. 12 for the Zγ channels, with the corresponding one-dimensional limits listed in Table 10 for Wγ, and Table 11 for Zγ.

Table 10: One-dimensional 95% CL limits on ATGCs for $W\gamma \to e\nu\gamma$, $W\gamma \to \mu\nu\gamma$, and for the combined analyses. The intervals shown represent the allowed ranges of the coupling parameters.

	$\Delta\kappa_\gamma$	λ_γ
$W\gamma \to e\nu\gamma$	$[-0.45, 0.36]$	$[-0.059, 0.046]$
$W\gamma \to \mu\nu\gamma$	$[-0.46, 0.34]$	$[-0.057, 0.045]$
$W\gamma \to \ell\nu\gamma$	$[-0.38, 0.29]$	$[-0.050, 0.037]$

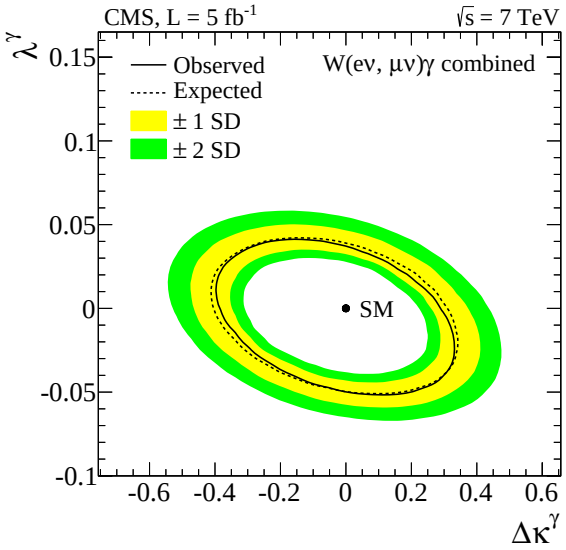

Figure 11: Observed (solid curve) and expected (dashed curve) 95% CL exclusion contours for anomalous WWγ couplings, with ±1 and ±2 standard deviation contours from uncertainties in the measurements indicated by light and dark shaded bands, respectively.

7 Summary

We have presented updated measurements of the Vγ inclusive production cross sections in pp collisions at $\sqrt{s} = 7$ TeV, based on leptonic decays of EW vector bosons $W \to e\nu$, $W \to \mu\nu$, $Z \to ee$, and $Z \to \mu\mu$. The data were collected by the CMS experiment at the LHC in 2011 and correspond to an integrated luminosity of $5.0\,\text{fb}^{-1}$. A separation is required between the photon and the charged leptons in (η, ϕ) space of $\Delta R > 0.7$, and an additional requirement

Table 11: One-dimensional 95% CL limits on ATGCs for $Z\gamma \to ee\gamma$, $Z\gamma \to \mu\mu\gamma$, and for the combined analyses. The intervals shown represent the allowed ranges of the coupling parameters.

	h_3^γ $[10^{-2}]$	h_4^γ $[10^{-4}]$	h_3^Z $[10^{-2}]$	h_4^Z $[10^{-4}]$
$Z\gamma \to ee\gamma$	$[-1.3, 1.3]$	$[-1.1, 1.1]$	$[-1.1, 1.1]$	$[-1.0, 1.0]$
$Z\gamma \to \mu\mu\gamma$	$[-1.3, 1.3]$	$[-1.1, 1.2]$	$[-1.1, 1.1]$	$[-1.0, 1.1]$
$Z\gamma \to \ell\ell\gamma$	$[-1.0, 1.0]$	$[-0.9, 0.9]$	$[-0.9, 0.9]$	$[-0.8, 0.8]$

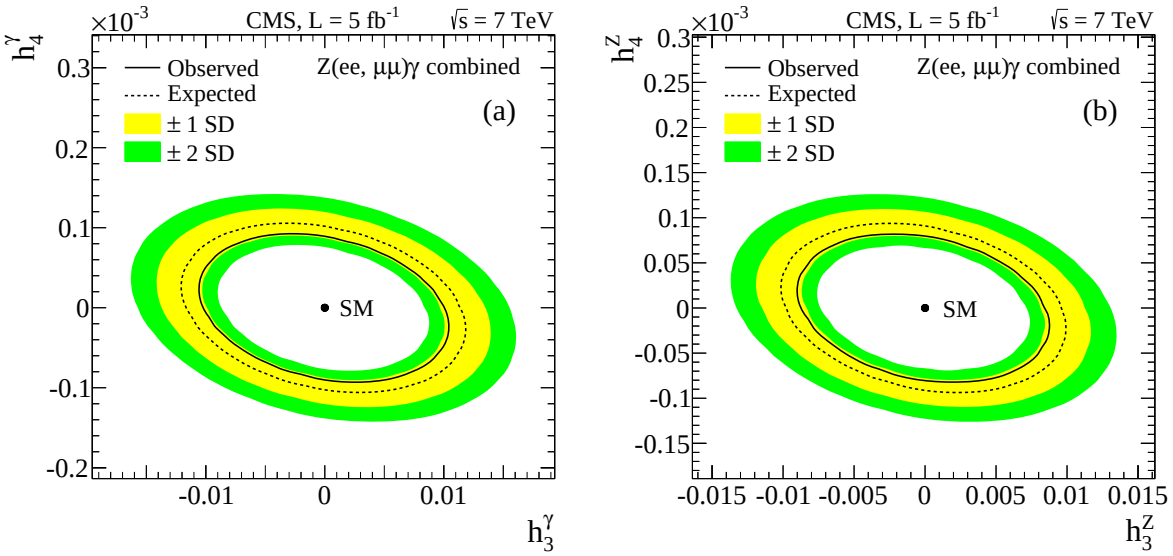

Figure 12: Observed (solid curves) and expected (dashed curves) 95% CL exclusion contours for anomalous (a) $Z\gamma\gamma$ and (b) $ZZ\gamma$ couplings, with ± 1 and ± 2 standard deviation contours indicated by light and dark shaded bands.

of $m_{\ell\ell} > 50\,\text{GeV}$ is placed on $Z\gamma$ candidates. The measured cross sections for $p_T^\gamma > 15\,\text{GeV}$, $\sigma(pp \to W\gamma) \times \mathcal{B}(W \to \ell\nu) = 37.0 \pm 0.8\,(\text{stat.}) \pm 4.0\,(\text{syst.}) \pm 0.8\,(\text{lum.})\,\text{pb}$ and $\sigma(pp \to Z\gamma) \times \mathcal{B}(Z \to \ell\ell) = 5.33 \pm 0.08\,(\text{stat.}) \pm 0.25\,(\text{syst.}) \pm 0.12\,(\text{lum.})\,\text{pb}$, are consistent with predictions of the SM; the ratio of these measurements, $6.9 \pm 0.2\,(\text{stat.}) \pm 0.5\,(\text{syst.})$, is also consistent with the SM value of 5.8 ± 0.1 predicted by MCFM. Measured cross sections for $p_T^\gamma > 60$ and >90 GeV also agree with the SM. With no evidence observed for physics beyond the SM, we set the limits on anomalous $WW\gamma$, $ZZ\gamma$, and $Z\gamma\gamma$ couplings given in Tables 10 and 11.

Acknowledgements

We congratulate our colleagues in the CERN accelerator departments for the excellent performance of the LHC and thank the technical and administrative staffs at CERN and at other CMS institutes for their contributions to the success of the CMS effort. In addition, we gratefully acknowledge the computing centers and personnel of the Worldwide LHC Computing Grid for delivering so effectively the computing infrastructure essential to our analyses. Finally, we acknowledge the enduring support for the construction and operation of the LHC and the CMS detector provided by the following funding agencies: the Austrian Federal Ministry of Science and Research and the Austrian Science Fund; the Belgian Fonds de la Recherche Scientifique, and Fonds voor Wetenschappelijk Onderzoek; the Brazilian Funding Agencies (CNPq, CAPES, FAPERJ, and FAPESP); the Bulgarian Ministry of Education, Youth and Science; CERN; the Chinese Academy of Sciences, Ministry of Science and Technology, and National Natural Science Foundation of China; the Colombian Funding Agency (COLCIENCIAS); the Croatian Ministry of Science, Education and Sport; the Research Promotion Foundation, Cyprus; the Ministry of Education and Research, Recurrent financing contract SF0690030s09 and European Regional Development Fund, Estonia; the Academy of Finland, Finnish Ministry of Education and Culture, and Helsinki Institute of Physics; the Institut National de Physique Nucléaire et de Physique des Particules / CNRS, and Commissariat à l'Énergie Atomique et aux Énergies Alternatives / CEA, France; the Bundesministerium für Bildung und Forschung, Deutsche Forschungsgemeinschaft, and Helmholtz-Gemeinschaft Deutscher Forschungszentren, Germany; the General Secretariat for Research and Technology, Greece; the National Scientific Research Foundation, and National Office for Research and Technology, Hungary; the Department of Atomic Energy and the Department of Science and Technology, India; the Institute for Studies in Theoretical Physics and Mathematics, Iran; the Science Foundation, Ireland; the Istituto Nazionale di Fisica Nucleare, Italy; the Korean Ministry of Education, Science and Technology and the World Class University program of NRF, Republic of Korea; the Lithuanian Academy of Sciences; the Mexican Funding Agencies (CINVESTAV, CONACYT, SEP, and UASLP-FAI); the Ministry of Science and Innovation, New Zealand; the Pakistan Atomic Energy Commission; the Ministry of Science and Higher Education and the National Science Centre, Poland; the Fundação para a Ciência e a Tecnologia, Portugal; JINR (Armenia, Belarus, Georgia, Ukraine, Uzbekistan); the Ministry of Education and Science of the Russian Federation, the Federal Agency of Atomic Energy of the Russian Federation, Russian Academy of Sciences, and the Russian Foundation for Basic Research; the Ministry of Science and Technological Development of Serbia; the Secretaría de Estado de Investigación, Desarrollo e Innovación and Programa Consolider-Ingenio 2010, Spain; the Swiss Funding Agencies (ETH Board, ETH Zurich, PSI, SNF, UniZH, Canton Zurich, and SER); the National Science Council, Taipei; the Thailand Center of Excellence in Physics, the Institute for the Promotion of Teaching Science and Technology of Thailand and the National Science and Technology Development Agency of Thailand; the Scientific and Technical Research Council of Turkey, and Turkish Atomic Energy Authority; the Science and Technology Facilities Council, UK; the US Department of Energy,

and the US National Science Foundation. Individuals have received support from the Marie-Curie programme and the European Research Council and EPLANET (European Union); the Leventis Foundation; the A. P. Sloan Foundation; the Alexander von Humboldt Foundation; the Belgian Federal Science Policy Office; the Fonds pour la Formation à la Recherche dans l'Industrie et dans l'Agriculture (FRIA-Belgium); the Agentschap voor Innovatie door Wetenschap en Technologie (IWT-Belgium); the Ministry of Education, Youth and Sports (MEYS) of Czech Republic; the Council of Science and Industrial Research, India; the Compagnia di San Paolo (Torino); and the HOMING PLUS programme of Foundation for Polish Science, cofinanced from European Union, Regional Development Fund.

References

[1] LEP Electroweak Working Group, "A Combination of Preliminary Electroweak Measurements and Constraints on the Standard Model", (2006). arXiv:hep-ex/0612034v2.

[2] L3 Collaboration, "Measurement of energetic single photon production at LEP", *Phys. Lett. B* **346** (1995) 190, doi:10.1016/0370-2693(95)00023-E.

[3] L3 Collaboration, "Study of the $e^+e^- \to Z\gamma$ process at LEP and limits on triple neutral-gauge-boson couplings", *Phys. Lett. B* **597** (2004) 119, doi:10.1016/j.physletb.2004.07.002.

[4] OPAL Collaboration, "Study of Z pair production and anomalous couplings in e^+e^- collisions at $\sqrt{s}$ between 190 GeV and 209 GeV", *Eur. Phys. J. C* **32** (2003) 303, doi:10.1140/epjc/s2003-01467-x.

[5] D0 Collaboration, "Measurement of $p\bar{p} \to W\gamma + X$ cross section at $\sqrt{s} = 1.96$ TeV and WWγ anomalous coupling limits", *Phys. Rev. D* **71** (2005) 091108, doi:10.1103/PhysRevD.71.091108.

[6] D0 Collaboration, "First Study of the Radiation-Amplitude Zero in Wγ Production and Limits on Anomalous WWγ Couplings at $\sqrt{s} = 1.96$ TeV", *Phys. Rev. Lett.* **100** (2008) 241805, doi:10.1103/PhysRevLett.100.241805.

[7] CDF Collaboration, "Measurement of $Z\gamma$ production in $p\bar{p}$ collisions at $\sqrt{s} = 1.96$ TeV", *Phys. Rev. D* **82** (2010) 031103, doi:10.1103/PhysRevD.82.031103.

[8] D0 Collaboration, "$Z\gamma$ production and limits on anomalous ZZγ and Z$\gamma\gamma$ couplings in $p\bar{p}$ collisions at $\sqrt{s} = 1.96$ TeV", *Phys. Lett. B* **653** (2007) 378, doi:10.1016/j.physletb.2007.08.035.

[9] D0 Collaboration, "Measurement of the $Z\gamma \to \nu\bar{\nu}\gamma$ Production Cross Section and Limits on Anomalous ZZγ and Z$\gamma\gamma$ Couplings in $p\bar{p}$ Collisions at $\sqrt{s} = 1.96$ TeV", *Phys. Rev. Lett.* **102** (2009) 201802, doi:10.1103/PhysRevLett.102.201802.

[10] CMS Collaboration, "Measurement of W^+W^- production and search for the Higgs boson in pp collisions at $\sqrt{s} = 7$ TeV", *Phys. Lett. B* **699** (2011) 25, doi:10.1016/j.physletb.2011.03.056.

[11] CMS Collaboration, "Measurement of Wγ and Zγ production in pp collisions at $\sqrt{s} = 7$ TeV", *Phys. Lett. B* **701** (2011) 535, doi:10.1016/j.physletb.2011.06.034.

[12] ATLAS Collaboration, "Measurement of Wγ and Zγ production in pp collisions at $\sqrt{s} = 7$ TeV with the ATLAS detector at the LHC", *Phys. Rev. D* **87** (2013) 112003, doi:10.1103/PhysRevD.87.112003.

[13] U. Baur, T. Han, and J. Ohnemus, "QCD corrections to hadronic Wγ production with nonstandard WWγ couplings", *Phys. Rev. D* **48** (1993) 5140, doi:10.1103/PhysRevD.48.5140.

[14] U. Baur, T. Han, and J. Ohnemus, "QCD corrections and anomalous couplings in Zγ production at hadron colliders", *Phys. Rev. D* **57** (1998) 2823, doi:10.1103/PhysRevD.57.2823.

[15] CMS Collaboration, "The CMS experiment at the CERN LHC", *JINST* **3** (2008) S08004, doi:10.1088/1748-0221/3/08/S08004.

[16] J. Alwall, M. Herquet, F. Maltoni, and O. Mattelaer, "MadGraph 5: Going Beyond", *JHEP* **06** (2011) 128, doi:10.1007/JHEP06(2011)128.

[17] T. Sjöstrand, S. Mrenna, and P. Z. Skands, "PYTHIA 6.4 physics and manual", *JHEP* **05** (2006) 26, doi:10.1088/1126-6708/2006/05/026, arXiv:hep-ph/0603175.

[18] T. Gleisberg et al., "Event generation with SHERPA 1.1", *JHEP* **02** (2009) 007, doi:10.1088/1126-6708/2009/02/007.

[19] J. Campbell, R. K. Ellis, and C. Williams, "Vector boson pair production at the LHC", *JHEP* **07** (2011) 018, doi:10.1007/JHEP07(2011)018.

[20] J. Campbell and R. K. Ellis, "Update on vector boson pair production at hadron colliders", *Phys. Rev. D* **60** (1999) 113006, doi:10.1103/PhysRevD.60.113006.

[21] P. M. Nadolsky et al., "Implications of CTEQ global analysis for collider observables", *Phys. Rev. D* **78** (2008) 013004, doi:10.1103/PhysRevD.78.013004.

[22] J. Pumplin et al., "New generation of parton distributions with uncertainties from global QCD analysis", *JHEP* **07** (2002) 012, doi:10.1088/1126-6708/2002/07/012, arXiv:hep-ph/0201195.

[23] GEANT4 Collaboration, "GEANT4—a simulation toolkit", *Nucl. Instrum. Meth. A* **506** (2003) 250, doi:10.1016/S0168-9002(03)01368-8.

[24] CMS Collaboration, "Performance of CMS muon reconstruction in pp collision events at $\sqrt{s}$ = 7 TeV", *JINST* **7** (2012) P10002, doi:10.1088/1748-0221/7/10/P10002.

[25] CMS Collaboration, "Measurement of the differential cross section for isolated prompt photon production in pp collisions at 7 TeV", *Phys. Rev. D* **84** (2011) 052011, doi:10.1103/PhysRevD.84.052011.

[26] M. Cacciari, G. Salam, and G. Soyez, "FastJet user manual", *Eur. Phys. J. C* **72** (2012) 1896, doi:10.1140/epjc/s10052-012-1896-2.

[27] CMS Collaboration, "Measurements of inclusive W and Z cross sections in pp collisions at $\sqrt{s} = 7$ TeV", *JHEP* **01** (2011) 080, doi:10.1007/JHEP01(2011)080.

[28] CMS Collaboration, "Observation of a new boson with mass near 125 GeV in pp collisions at $\sqrt{s} = 7$ and 8 TeV", *JHEP* **06** (2013) 081, doi:10.1007/JHEP06(2013)081.

[29] CMS Collaboration, "Commissioning of the particle-flow event reconstruction with leptons from J/ψ and W decays at 7 TeV", CMS Physics Analysis Summary CMS-PAS-PFT-10-003, (2010).

[30] K. Cranmer, "Kernel estimation in high-energy physics", *Comput. Phys. Commun.* **136** (2001) 198, doi:10.1016/S0010-4655(00)00243-5.

[31] T. Skwarnicki, "A study of the radiative cascade transitions between the upsilon-prime and upsilon resonances". PhD thesis, 1986. DESY internal report DESY-F31-86-02.

[32] R. W. Brown, D. Sahdev, and K. O. Mikaelian, "$W^{\pm}Z^0$ and $W^{\pm}\gamma$ pair production in νe, pp, and $\bar{p}p$ collisions", *Phys. Rev. D* **20** (1979) 1164, doi:10.1103/PhysRevD.20.1164.

[33] K. O. Mikaelian, M. A. Samuel, and D. Sahdev, "Magnetic Moment of Weak Bosons Produced in pp and $p\bar{p}$ Collisions", *Phys. Rev. Lett.* **43** (1979) 746, doi:10.1103/PhysRevLett.43.746.

[34] C. J. Goebel, F. Halzen, and J. P. Leveille, "Angular zeros of Brown, Mikaelian, Sahdev, and Samuel and the factorization of tree amplitudes in gauge theories", *Phys. Rev. D* **23** (1981) 2682, doi:10.1103/PhysRevD.23.2682.

[35] S. J. Brodsky and R. W. Brown, "Zeros in Amplitude: Gauge Theory and Radiation Interference", *Phys. Rev. Lett.* **49** (1982) 966, doi:10.1103/PhysRevLett.49.966.

[36] R. W. Brown, K. L. Kowalski, and S. J. Brodsky, "Classical radiation zeros in gauge-theory amplitudes", *Phys. Rev. D* **28** (1983) 624, doi:10.1103/PhysRevD.28.624.

[37] U. Baur, S. Errede, and G. Landsberg, "Rapidity correlations in Wγ production at hadron colliders", *Phys. Rev. D* **50** (1994) 1917, doi:10.1103/PhysRevD.50.1917.

[38] CMS Collaboration, "Search for the standard model Higgs boson decaying into two photons in pp collisions at $\sqrt{s} = 7$ TeV", *Phys. Lett. B* **710** (2012) 403, doi:10.1016/j.physletb.2012.03.003.

[39] CMS Collaboration, "Measurement of the inelastic proton-proton cross section at $\sqrt{s} = 7$ TeV", *Phys. Lett. B* **722** (2013) 5, doi:10.1016/j.physletb.2013.03.024.

[40] CMS Collaboration, "Absolute Calibration of the Luminosity Measurement at CMS: Winter 2012 Update", CMS Physics Analysis Summary CMS-PAS-SMP-12-008, (2012).

[41] L. Lyons, G. Gibaut, and P. Clifford, "How to combine correlated estimates of a single physical quantity", *Nucl. Instrum. Meth. A* **270** (1988) 110, doi:10.1016/0168-9002(88)90018-6.

[42] K. Hagiwara, R. D. Peccei, and D. Zeppenfeld, "Probing the weak boson sector in $e^+e^- \to W^+W^-$", *Nucl. Phys. B* **282** (1987) 253, doi:10.1016/0550-3213(87)90685-7.

[43] K. Hagiwara, J. Woodside, and D. Zeppenfeld, "Measuring the WWZ coupling at the Fermilab Tevatron", *Phys. Rev. D* **41** (1990) 2113, doi:10.1103/PhysRevD.41.2113.

[44] U. Baur and E. Berger, "Probing the weak-boson sector in $Z\gamma$ production at hadron colliders", *Phys. Rev. D* **47** (1993) 4889, doi:10.1103/PhysRevD.47.4889.

[45] G. Cowan, K. Cranmer, E. Gross, and O. Vitells, "Asymptotic formulae for likelihood-based tests of new physics", *Eur. Phys. J. C* **71** (2011) 1554, doi:10.1140/epjc/s10052-011-1554-0.

[46] G. Gounaris, J.-L. Kneur, D. Zeppenfeld et al., "Triple gauge boson couplings", in *Physics at LEP2*, volume 1, p. 525. 1996. arXiv:hep-ph/9601233. doi:10.5170/CERN-1996-001-V-1.

A The CMS Collaboration

Yerevan Physics Institute, Yerevan, Armenia
S. Chatrchyan, V. Khachatryan, A.M. Sirunyan, A. Tumasyan

Institut für Hochenergiephysik der OeAW, Wien, Austria
W. Adam, T. Bergauer, M. Dragicevic, J. Erö, C. Fabjan[1], M. Friedl, R. Frühwirth[1], V.M. Ghete, N. Hörmann, J. Hrubec, M. Jeitler[1], W. Kiesenhofer, V. Knünz, M. Krammer[1], I. Krätschmer, D. Liko, I. Mikulec, D. Rabady[2], B. Rahbaran, C. Rohringer, H. Rohringer, R. Schöfbeck, J. Strauss, A. Taurok, W. Treberer-Treberspurg, W. Waltenberger, C.-E. Wulz[1]

National Centre for Particle and High Energy Physics, Minsk, Belarus
V. Mossolov, N. Shumeiko, J. Suarez Gonzalez

Universiteit Antwerpen, Antwerpen, Belgium
S. Alderweireldt, M. Bansal, S. Bansal, T. Cornelis, E.A. De Wolf, X. Janssen, A. Knutsson, S. Luyckx, L. Mucibello, S. Ochesanu, B. Roland, R. Rougny, Z. Staykova, H. Van Haevermaet, P. Van Mechelen, N. Van Remortel, A. Van Spilbeeck

Vrije Universiteit Brussel, Brussel, Belgium
F. Blekman, S. Blyweert, J. D'Hondt, A. Kalogeropoulos, J. Keaveney, M. Maes, A. Olbrechts, S. Tavernier, W. Van Doninck, P. Van Mulders, G.P. Van Onsem, I. Villella

Université Libre de Bruxelles, Bruxelles, Belgium
B. Clerbaux, G. De Lentdecker, L. Favart, A.P.R. Gay, T. Hreus, A. Léonard, P.E. Marage, A. Mohammadi, L. Perniè, T. Reis, T. Seva, L. Thomas, C. Vander Velde, P. Vanlaer, J. Wang

Ghent University, Ghent, Belgium
V. Adler, K. Beernaert, L. Benucci, A. Cimmino, S. Costantini, S. Dildick, G. Garcia, B. Klein, J. Lellouch, A. Marinov, J. Mccartin, A.A. Ocampo Rios, D. Ryckbosch, M. Sigamani, N. Strobbe, F. Thyssen, M. Tytgat, S. Walsh, E. Yazgan, N. Zaganidis

Université Catholique de Louvain, Louvain-la-Neuve, Belgium
S. Basegmez, C. Beluffi[3], G. Bruno, R. Castello, A. Caudron, L. Ceard, C. Delaere, T. du Pree, D. Favart, L. Forthomme, A. Giammanco[4], J. Hollar, P. Jez, V. Lemaitre, J. Liao, O. Militaru, C. Nuttens, D. Pagano, A. Pin, K. Piotrzkowski, A. Popov[5], M. Selvaggi, J.M. Vizan Garcia

Université de Mons, Mons, Belgium
N. Beliy, T. Caebergs, E. Daubie, G.H. Hammad

Centro Brasileiro de Pesquisas Fisicas, Rio de Janeiro, Brazil
G.A. Alves, M. Correa Martins Junior, T. Martins, M.E. Pol, M.H.G. Souza

Universidade do Estado do Rio de Janeiro, Rio de Janeiro, Brazil
W.L. Aldá Júnior, W. Carvalho, J. Chinellato[6], A. Custódio, E.M. Da Costa, D. De Jesus Damiao, C. De Oliveira Martins, S. Fonseca De Souza, H. Malbouisson, M. Malek, D. Matos Figueiredo, L. Mundim, H. Nogima, W.L. Prado Da Silva, A. Santoro, A. Sznajder, E.J. Tonelli Manganote[6], A. Vilela Pereira

Universidade Estadual Paulista [a], Universidade Federal do ABC [b], São Paulo, Brazil
C.A. Bernardes[b], F.A. Dias[a,7], T.R. Fernandez Perez Tomei[a], E.M. Gregores[b], C. Lagana[a], P.G. Mercadante[b], S.F. Novaes[a], Sandra S. Padula[a]

Institute for Nuclear Research and Nuclear Energy, Sofia, Bulgaria
V. Genchev[2], P. Iaydjiev[2], S. Piperov, M. Rodozov, G. Sultanov, M. Vutova

University of Sofia, Sofia, Bulgaria
A. Dimitrov, R. Hadjiiska, V. Kozhuharov, L. Litov, B. Pavlov, P. Petkov

Institute of High Energy Physics, Beijing, China
J.G. Bian, G.M. Chen, H.S. Chen, C.H. Jiang, D. Liang, S. Liang, X. Meng, J. Tao, J. Wang, X. Wang, Z. Wang, H. Xiao, M. Xu

State Key Laboratory of Nuclear Physics and Technology, Peking University, Beijing, China
C. Asawatangtrakuldee, Y. Ban, Y. Guo, Q. Li, W. Li, S. Liu, Y. Mao, S.J. Qian, D. Wang, L. Zhang, W. Zou

Universidad de Los Andes, Bogota, Colombia
C. Avila, C.A. Carrillo Montoya, L.F. Chaparro Sierra, J.P. Gomez, B. Gomez Moreno, J.C. Sanabria

Technical University of Split, Split, Croatia
N. Godinovic, D. Lelas, R. Plestina[8], D. Polic, I. Puljak

University of Split, Split, Croatia
Z. Antunovic, M. Kovac

Institute Rudjer Boskovic, Zagreb, Croatia
V. Brigljevic, S. Duric, K. Kadija, J. Luetic, D. Mekterovic, S. Morovic, L. Tikvica

University of Cyprus, Nicosia, Cyprus
A. Attikis, G. Mavromanolakis, J. Mousa, C. Nicolaou, F. Ptochos, P.A. Razis

Charles University, Prague, Czech Republic
M. Finger, M. Finger Jr.

Academy of Scientific Research and Technology of the Arab Republic of Egypt, Egyptian Network of High Energy Physics, Cairo, Egypt
A.A. Abdelalim[9], Y. Assran[10], S. Elgammal[9], A. Ellithi Kamel[11], M.A. Mahmoud[12], A. Radi[13,14]

National Institute of Chemical Physics and Biophysics, Tallinn, Estonia
M. Kadastik, M. Müntel, M. Murumaa, M. Raidal, L. Rebane, A. Tiko

Department of Physics, University of Helsinki, Helsinki, Finland
P. Eerola, G. Fedi, M. Voutilainen

Helsinki Institute of Physics, Helsinki, Finland
J. Härkönen, V. Karimäki, R. Kinnunen, M.J. Kortelainen, T. Lampén, K. Lassila-Perini, S. Lehti, T. Lindén, P. Luukka, T. Mäenpää, T. Peltola, E. Tuominen, J. Tuominiemi, E. Tuovinen, L. Wendland

Lappeenranta University of Technology, Lappeenranta, Finland
T. Tuuva

DSM/IRFU, CEA/Saclay, Gif-sur-Yvette, France
M. Besancon, F. Couderc, M. Dejardin, D. Denegri, B. Fabbro, J.L. Faure, F. Ferri, S. Ganjour, A. Givernaud, P. Gras, G. Hamel de Monchenault, P. Jarry, E. Locci, J. Malcles, L. Millischer, A. Nayak, J. Rander, A. Rosowsky, M. Titov

Laboratoire Leprince-Ringuet, Ecole Polytechnique, IN2P3-CNRS, Palaiseau, France
S. Baffioni, F. Beaudette, L. Benhabib, M. Bluj[15], P. Busson, C. Charlot, N. Daci, T. Dahms, M. Dalchenko, L. Dobrzynski, A. Florent, R. Granier de Cassagnac, M. Haguenauer, P. Miné,

C. Mironov, I.N. Naranjo, M. Nguyen, C. Ochando, P. Paganini, D. Sabes, R. Salerno, Y. Sirois, C. Veelken, A. Zabi

Institut Pluridisciplinaire Hubert Curien, Université de Strasbourg, Université de Haute Alsace Mulhouse, CNRS/IN2P3, Strasbourg, France
J.-L. Agram[16], J. Andrea, D. Bloch, J.-M. Brom, E.C. Chabert, C. Collard, E. Conte[16], F. Drouhin[16], J.-C. Fontaine[16], D. Gelé, U. Goerlach, C. Goetzmann, P. Juillot, A.-C. Le Bihan, P. Van Hove

Centre de Calcul de l'Institut National de Physique Nucleaire et de Physique des Particules, CNRS/IN2P3, Villeurbanne, France
S. Gadrat

Université de Lyon, Université Claude Bernard Lyon 1, CNRS-IN2P3, Institut de Physique Nucléaire de Lyon, Villeurbanne, France
S. Beauceron, N. Beaupere, G. Boudoul, S. Brochet, J. Chasserat, R. Chierici, D. Contardo, P. Depasse, H. El Mamouni, J. Fay, S. Gascon, M. Gouzevitch, B. Ille, T. Kurca, M. Lethuillier, L. Mirabito, S. Perries, L. Sgandurra, V. Sordini, Y. Tschudi, M. Vander Donckt, P. Verdier, S. Viret

Institute of High Energy Physics and Informatization, Tbilisi State University, Tbilisi, Georgia
Z. Tsamalaidze[17]

RWTH Aachen University, I. Physikalisches Institut, Aachen, Germany
C. Autermann, S. Beranek, B. Calpas, M. Edelhoff, L. Feld, N. Heracleous, O. Hindrichs, K. Klein, A. Ostapchuk, A. Perieanu, F. Raupach, J. Sammet, S. Schael, D. Sprenger, H. Weber, B. Wittmer, V. Zhukov[5]

RWTH Aachen University, III. Physikalisches Institut A, Aachen, Germany
M. Ata, J. Caudron, E. Dietz-Laursonn, D. Duchardt, M. Erdmann, R. Fischer, A. Güth, T. Hebbeker, C. Heidemann, K. Hoepfner, D. Klingebiel, P. Kreuzer, M. Merschmeyer, A. Meyer, M. Olschewski, K. Padeken, P. Papacz, H. Pieta, H. Reithler, S.A. Schmitz, L. Sonnenschein, J. Steggemann, D. Teyssier, S. Thüer, M. Weber

RWTH Aachen University, III. Physikalisches Institut B, Aachen, Germany
V. Cherepanov, Y. Erdogan, G. Flügge, H. Geenen, M. Geisler, W. Haj Ahmad, F. Hoehle, B. Kargoll, T. Kress, Y. Kuessel, J. Lingemann[2], A. Nowack, I.M. Nugent, L. Perchalla, O. Pooth, A. Stahl

Deutsches Elektronen-Synchrotron, Hamburg, Germany
M. Aldaya Martin, I. Asin, N. Bartosik, J. Behr, W. Behrenhoff, U. Behrens, M. Bergholz[18], A. Bethani, K. Borras, A. Burgmeier, A. Cakir, L. Calligaris, A. Campbell, S. Choudhury, F. Costanza, C. Diez Pardos, S. Dooling, T. Dorland, G. Eckerlin, D. Eckstein, G. Flucke, A. Geiser, I. Glushkov, P. Gunnellini, S. Habib, J. Hauk, G. Hellwig, D. Horton, H. Jung, M. Kasemann, P. Katsas, C. Kleinwort, H. Kluge, M. Krämer, D. Krücker, E. Kuznetsova, W. Lange, J. Leonard, K. Lipka, W. Lohmann[18], B. Lutz, R. Mankel, I. Marfin, I.-A. Melzer-Pellmann, A.B. Meyer, J. Mnich, A. Mussgiller, S. Naumann-Emme, O. Novgorodova, F. Nowak, J. Olzem, H. Perrey, A. Petrukhin, D. Pitzl, R. Placakyte, A. Raspereza, P.M. Ribeiro Cipriano, C. Riedl, E. Ron, M.Ö. Sahin, J. Salfeld-Nebgen, R. Schmidt[18], T. Schoerner-Sadenius, N. Sen, M. Stein, R. Walsh, C. Wissing

University of Hamburg, Hamburg, Germany
V. Blobel, H. Enderle, J. Erfle, E. Garutti, U. Gebbert, M. Görner, M. Gosselink, J. Haller,

K. Heine, R.S. Höing, G. Kaussen, H. Kirschenmann, R. Klanner, R. Kogler, J. Lange, I. Marchesini, T. Peiffer, N. Pietsch, D. Rathjens, C. Sander, H. Schettler, P. Schleper, E. Schlieckau, A. Schmidt, M. Schröder, T. Schum, M. Seidel, J. Sibille[19], V. Sola, H. Stadie, G. Steinbrück, J. Thomsen, D. Troendle, E. Usai, L. Vanelderen

Institut für Experimentelle Kernphysik, Karlsruhe, Germany
C. Barth, C. Baus, J. Berger, C. Böser, E. Butz, T. Chwalek, W. De Boer, A. Descroix, A. Dierlamm, M. Feindt, M. Guthoff[2], F. Hartmann[2], T. Hauth[2], H. Held, K.H. Hoffmann, U. Husemann, I. Katkov[5], J.R. Komaragiri, A. Kornmayer[2], P. Lobelle Pardo, D. Martschei, Th. Müller, M. Niegel, A. Nürnberg, O. Oberst, J. Ott, G. Quast, K. Rabbertz, F. Ratnikov, S. Röcker, F.-P. Schilling, G. Schott, H.J. Simonis, F.M. Stober, R. Ulrich, J. Wagner-Kuhr, S. Wayand, T. Weiler, M. Zeise

Institute of Nuclear and Particle Physics (INPP), NCSR Demokritos, Aghia Paraskevi, Greece
G. Anagnostou, G. Daskalakis, T. Geralis, S. Kesisoglou, A. Kyriakis, D. Loukas, A. Markou, C. Markou, E. Ntomari

University of Athens, Athens, Greece
L. Gouskos, A. Panagiotou, N. Saoulidou, E. Stiliaris

University of Ioánnina, Ioánnina, Greece
X. Aslanoglou, I. Evangelou, G. Flouris, C. Foudas, P. Kokkas, N. Manthos, I. Papadopoulos, E. Paradas

KFKI Research Institute for Particle and Nuclear Physics, Budapest, Hungary
G. Bencze, C. Hajdu, P. Hidas, D. Horvath[20], B. Radics, F. Sikler, V. Veszpremi, G. Vesztergombi[21], A.J. Zsigmond

Institute of Nuclear Research ATOMKI, Debrecen, Hungary
N. Beni, S. Czellar, J. Molnar, J. Palinkas, Z. Szillasi

University of Debrecen, Debrecen, Hungary
J. Karancsi, P. Raics, Z.L. Trocsanyi, B. Ujvari

National Institute of Science Education and Research, Bhubaneswar, India
S.K. Swain[22]

Panjab University, Chandigarh, India
S.B. Beri, V. Bhatnagar, N. Dhingra, R. Gupta, M. Kaur, M.Z. Mehta, M. Mittal, N. Nishu, L.K. Saini, A. Sharma, J.B. Singh

University of Delhi, Delhi, India
Ashok Kumar, Arun Kumar, S. Ahuja, A. Bhardwaj, B.C. Choudhary, S. Malhotra, M. Naimuddin, K. Ranjan, P. Saxena, V. Sharma, R.K. Shivpuri

Saha Institute of Nuclear Physics, Kolkata, India
S. Banerjee, S. Bhattacharya, K. Chatterjee, S. Dutta, B. Gomber, Sa. Jain, Sh. Jain, R. Khurana, A. Modak, S. Mukherjee, D. Roy, S. Sarkar, M. Sharan, A.P. Singh

Bhabha Atomic Research Centre, Mumbai, India
A. Abdulsalam, D. Dutta, S. Kailas, V. Kumar, A.K. Mohanty[2], L.M. Pant, P. Shukla, A. Topkar

Tata Institute of Fundamental Research - EHEP, Mumbai, India
T. Aziz, R.M. Chatterjee, S. Ganguly, S. Ghosh, M. Guchait[23], A. Gurtu[24], G. Kole,

S. Kumar, M. Maity[25], G. Majumder, K. Mazumdar, G.B. Mohanty, B. Parida, K. Sudhakar, N. Wickramage[26]

Tata Institute of Fundamental Research - HECR, Mumbai, India
S. Banerjee, S. Dugad

Institute for Research in Fundamental Sciences (IPM), Tehran, Iran
H. Arfaei, H. Bakhshiansohi, S.M. Etesami[27], A. Fahim[28], H. Hesari, A. Jafari, M. Khakzad, M. Mohammadi Najafabadi, S. Paktinat Mehdiabadi, B. Safarzadeh[29], M. Zeinali

University College Dublin, Dublin, Ireland
M. Grunewald

INFN Sezione di Bari [a], Università di Bari [b], Politecnico di Bari [c], Bari, Italy
M. Abbrescia[a,b], L. Barbone[a,b], C. Calabria[a,b], S.S. Chhibra[a,b], A. Colaleo[a], D. Creanza[a,c], N. De Filippis[a,c], M. De Palma[a,b], L. Fiore[a], G. Iaselli[a,c], G. Maggi[a,c], M. Maggi[a], B. Marangelli[a,b], S. My[a,c], S. Nuzzo[a,b], N. Pacifico[a], A. Pompili[a,b], G. Pugliese[a,c], G. Selvaggi[a,b], L. Silvestris[a], G. Singh[a,b], R. Venditti[a,b], P. Verwilligen[a], G. Zito[a]

INFN Sezione di Bologna [a], Università di Bologna [b], Bologna, Italy
G. Abbiendi[a], A.C. Benvenuti[a], D. Bonacorsi[a,b], S. Braibant-Giacomelli[a,b], L. Brigliadori[a,b], R. Campanini[a,b], P. Capiluppi[a,b], A. Castro[a,b], F.R. Cavallo[a], G. Codispoti, M. Cuffiani[a,b], G.M. Dallavalle[a], F. Fabbri[a], A. Fanfani[a,b], D. Fasanella[a,b], P. Giacomelli[a], C. Grandi[a], L. Guiducci[a,b], S. Marcellini[a], G. Masetti[a,2], M. Meneghelli[a,b], A. Montanari[a], F.L. Navarria[a,b], F. Odorici[a], A. Perrotta[a], F. Primavera[a,b], A.M. Rossi[a,b], T. Rovelli[a,b], G.P. Siroli[a,b], N. Tosi[a,b], R. Travaglini[a,b]

INFN Sezione di Catania [a], Università di Catania [b], Catania, Italy
S. Albergo[a,b], M. Chiorboli[a,b], S. Costa[a,b], F. Giordano[a,2], R. Potenza[a,b], A. Tricomi[a,b], C. Tuve[a,b]

INFN Sezione di Firenze [a], Università di Firenze [b], Firenze, Italy
G. Barbagli[a], V. Ciulli[a,b], C. Civinini[a], R. D'Alessandro[a,b], E. Focardi[a,b], S. Frosali[a,b], E. Gallo[a], S. Gonzi[a,b], V. Gori[a,b], P. Lenzi[a,b], M. Meschini[a], S. Paoletti[a], G. Sguazzoni[a], A. Tropiano[a,b]

INFN Laboratori Nazionali di Frascati, Frascati, Italy
L. Benussi, S. Bianco, F. Fabbri, D. Piccolo

INFN Sezione di Genova [a], Università di Genova [b], Genova, Italy
P. Fabbricatore[a], R. Musenich[a], S. Tosi[a,b]

INFN Sezione di Milano-Bicocca [a], Università di Milano-Bicocca [b], Milano, Italy
A. Benaglia[a], F. De Guio[a,b], M.E. Dinardo, S. Fiorendi[a,b], S. Gennai[a], A. Ghezzi[a,b], P. Govoni, M.T. Lucchini[2], S. Malvezzi[a], R.A. Manzoni[a,b,2], A. Martelli[a,b,2], D. Menasce[a], L. Moroni[a], M. Paganoni[a,b], D. Pedrini[a], S. Ragazzi[a,b], N. Redaelli[a], T. Tabarelli de Fatis[a,b]

INFN Sezione di Napoli [a], Università di Napoli 'Federico II' [b], Università della Basilicata (Potenza) [c], Università G. Marconi (Roma) [d], Napoli, Italy
S. Buontempo[a], N. Cavallo[a,c], A. De Cosa[a,b], F. Fabozzi[a,c], A.O.M. Iorio[a,b], L. Lista[a], S. Meola[a,d,2], M. Merola[a], P. Paolucci[a,2]

INFN Sezione di Padova [a], Università di Padova [b], Università di Trento (Trento) [c], Padova, Italy
P. Azzi[a], N. Bacchetta[a], D. Bisello[a,b], A. Branca[a,b], R. Carlin[a,b], P. Checchia[a], T. Dorigo[a], U. Dosselli[a], F. Fanzago[a], M. Galanti[a,b,2], F. Gasparini[a,b], U. Gasparini[a,b], P. Giubilato[a,b], A. Gozzelino[a], K. Kanishchev[a,c], S. Lacaprara[a], I. Lazzizzera[a,c], M. Margoni[a,b],

A.T. Meneguzzo[a,b], M. Passaseo[a], J. Pazzini[a,b], M. Pegoraro[a], N. Pozzobon[a,b], P. Ronchese[a,b], M. Sgaravatto[a], F. Simonetto[a,b], E. Torassa[a], M. Tosi[a,b], P. Zotto[a,b], G. Zumerle[a,b]

INFN Sezione di Pavia [a], Università di Pavia [b], Pavia, Italy
M. Gabusi[a,b], S.P. Ratti[a,b], C. Riccardi[a,b], P. Vitulo[a,b]

INFN Sezione di Perugia [a], Università di Perugia [b], Perugia, Italy
M. Biasini[a,b], G.M. Bilei[a], L. Fanò[a,b], P. Lariccia[a,b], G. Mantovani[a,b], M. Menichelli[a], A. Nappi[a,b†], F. Romeo[a,b], A. Saha[a], A. Santocchia[a,b], A. Spiezia[a,b]

INFN Sezione di Pisa [a], Università di Pisa [b], Scuola Normale Superiore di Pisa [c], Pisa, Italy
K. Androsov[a,30], P. Azzurri[a], G. Bagliesi[a], J. Bernardini[a], T. Boccali[a], G. Broccolo[a,c], R. Castaldi[a], R.T. D'Agnolo[a,c,2], R. Dell'Orso[a], F. Fiori[a,c], L. Foà[a,c], A. Giassi[a], M.T. Grippo[a,30], A. Kraan[a], F. Ligabue[a,c], T. Lomtadze[a], L. Martini[a,30], A. Messineo[a,b], F. Palla[a], A. Rizzi[a,b], A. Savoy-Navarro[a,31], A.T. Serban[a], P. Spagnolo[a], P. Squillacioti[a], R. Tenchini[a], G. Tonelli[a,b], A. Venturi[a], P.G. Verdini[a], C. Vernieri[a,c]

INFN Sezione di Roma [a], Università di Roma [b], Roma, Italy
L. Barone[a,b], F. Cavallari[a], D. Del Re[a,b], M. Diemoz[a], M. Grassi[a,b], E. Longo[a,b], F. Margaroli[a,b], P. Meridiani[a], F. Micheli[a,b], S. Nourbakhsh[a,b], G. Organtini[a,b], R. Paramatti[a], S. Rahatlou[a,b], C. Rovelli[a], L. Soffi[a,b]

INFN Sezione di Torino [a], Università di Torino [b], Università del Piemonte Orientale (Novara) [c], Torino, Italy
N. Amapane[a,b], R. Arcidiacono[a,c], S. Argiro[a,b], M. Arneodo[a,c], C. Biino[a], N. Cartiglia[a], S. Casasso[a,b], M. Costa[a,b], N. Demaria[a], C. Mariotti[a], S. Maselli[a], E. Migliore[a,b], V. Monaco[a,b], M. Musich[a], M.M. Obertino[a,c], G. Ortona[a,b], N. Pastrone[a], M. Pelliccioni[a,2], A. Potenza[a,b], A. Romero[a,b], M. Ruspa[a,c], R. Sacchi[a,b], A. Solano[a,b], A. Staiano[a], U. Tamponi[a]

INFN Sezione di Trieste [a], Università di Trieste [b], Trieste, Italy
S. Belforte[a], V. Candelise[a,b], M. Casarsa[a], F. Cossutti[a,2], G. Della Ricca[a,b], B. Gobbo[a], C. La Licata[a,b], M. Marone[a,b], D. Montanino[a,b], A. Penzo[a], A. Schizzi[a,b], A. Zanetti[a]

Kangwon National University, Chunchon, Korea
S. Chang, T.Y. Kim, S.K. Nam

Kyungpook National University, Daegu, Korea
D.H. Kim, G.N. Kim, J.E. Kim, D.J. Kong, Y.D. Oh, H. Park, D.C. Son

Chonnam National University, Institute for Universe and Elementary Particles, Kwangju, Korea
J.Y. Kim, Zero J. Kim, S. Song

Korea University, Seoul, Korea
S. Choi, D. Gyun, B. Hong, M. Jo, H. Kim, T.J. Kim, K.S. Lee, S.K. Park, Y. Roh

University of Seoul, Seoul, Korea
M. Choi, J.H. Kim, C. Park, I.C. Park, S. Park, G. Ryu

Sungkyunkwan University, Suwon, Korea
Y. Choi, Y.K. Choi, J. Goh, M.S. Kim, E. Kwon, B. Lee, J. Lee, S. Lee, H. Seo, I. Yu

Vilnius University, Vilnius, Lithuania
I. Grigelionis, A. Juodagalvis

Centro de Investigacion y de Estudios Avanzados del IPN, Mexico City, Mexico
H. Castilla-Valdez, E. De La Cruz-Burelo, I. Heredia-de La Cruz[32], R. Lopez-Fernandez, J. Martínez-Ortega, A. Sanchez-Hernandez, L.M. Villasenor-Cendejas

Universidad Iberoamericana, Mexico City, Mexico
S. Carrillo Moreno, F. Vazquez Valencia

Benemerita Universidad Autonoma de Puebla, Puebla, Mexico
H.A. Salazar Ibarguen

Universidad Autónoma de San Luis Potosí, San Luis Potosí, Mexico
E. Casimiro Linares, A. Morelos Pineda, M.A. Reyes-Santos

University of Auckland, Auckland, New Zealand
D. Krofcheck

University of Canterbury, Christchurch, New Zealand
A.J. Bell, P.H. Butler, R. Doesburg, S. Reucroft, H. Silverwood

National Centre for Physics, Quaid-I-Azam University, Islamabad, Pakistan
M. Ahmad, M.I. Asghar, J. Butt, H.R. Hoorani, S. Khalid, W.A. Khan, T. Khurshid, S. Qazi, M.A. Shah, M. Shoaib

National Centre for Nuclear Research, Swierk, Poland
H. Bialkowska, B. Boimska, T. Frueboes, M. Górski, M. Kazana, K. Nawrocki, K. Romanowska-Rybinska, M. Szleper, G. Wrochna, P. Zalewski

Institute of Experimental Physics, Faculty of Physics, University of Warsaw, Warsaw, Poland
G. Brona, K. Bunkowski, M. Cwiok, W. Dominik, K. Doroba, A. Kalinowski, M. Konecki, J. Krolikowski, M. Misiura, W. Wolszczak

Laboratório de Instrumentação e Física Experimental de Partículas, Lisboa, Portugal
N. Almeida, P. Bargassa, C. Beirão Da Cruz E Silva, P. Faccioli, P.G. Ferreira Parracho, M. Gallinaro, F. Nguyen, J. Rodrigues Antunes, J. Seixas[2], J. Varela, P. Vischia

Joint Institute for Nuclear Research, Dubna, Russia
S. Afanasiev, P. Bunin, I. Golutvin, I. Gorbunov, A. Kamenev, V. Karjavin, V. Konoplyanikov, G. Kozlov, A. Lanev, A. Malakhov, V. Matveev, P. Moisenz, V. Palichik, V. Perelygin, S. Shmatov, N. Skatchkov, V. Smirnov, A. Zarubin

Petersburg Nuclear Physics Institute, Gatchina (St. Petersburg), Russia
S. Evstyukhin, V. Golovtsov, Y. Ivanov, V. Kim, P. Levchenko, V. Murzin, V. Oreshkin, I. Smirnov, V. Sulimov, L. Uvarov, S. Vavilov, A. Vorobyev, An. Vorobyev

Institute for Nuclear Research, Moscow, Russia
Yu. Andreev, A. Dermenev, S. Gninenko, N. Golubev, M. Kirsanov, N. Krasnikov, A. Pashenkov, D. Tlisov, A. Toropin

Institute for Theoretical and Experimental Physics, Moscow, Russia
V. Epshteyn, M. Erofeeva, V. Gavrilov, N. Lychkovskaya, V. Popov, G. Safronov, S. Semenov, A. Spiridonov, V. Stolin, E. Vlasov, A. Zhokin

P.N. Lebedev Physical Institute, Moscow, Russia
V. Andreev, M. Azarkin, I. Dremin, M. Kirakosyan, A. Leonidov, G. Mesyats, S.V. Rusakov, A. Vinogradov

Skobeltsyn Institute of Nuclear Physics, Lomonosov Moscow State University, Moscow, Russia
A. Belyaev, E. Boos, V. Bunichev, M. Dubinin[7], L. Dudko, A. Gribushin, V. Klyukhin, O. Kodolova, I. Lokhtin, A. Markina, S. Obraztsov, S. Petrushanko, V. Savrin, A. Snigirev

State Research Center of Russian Federation, Institute for High Energy Physics, Protvino, Russia
I. Azhgirey, I. Bayshev, S. Bitioukov, V. Kachanov, A. Kalinin, D. Konstantinov, V. Krychkine, V. Petrov, R. Ryutin, A. Sobol, L. Tourtchanovitch, S. Troshin, N. Tyurin, A. Uzunian, A. Volkov

University of Belgrade, Faculty of Physics and Vinca Institute of Nuclear Sciences, Belgrade, Serbia
P. Adzic[33], M. Djordjevic, M. Ekmedzic, D. Krpic[33], J. Milosevic

Centro de Investigaciones Energéticas Medioambientales y Tecnológicas (CIEMAT), Madrid, Spain
M. Aguilar-Benitez, J. Alcaraz Maestre, C. Battilana, E. Calvo, M. Cerrada, M. Chamizo Llatas[2], N. Colino, B. De La Cruz, A. Delgado Peris, D. Domínguez Vázquez, C. Fernandez Bedoya, J.P. Fernández Ramos, A. Ferrando, J. Flix, M.C. Fouz, P. Garcia-Abia, O. Gonzalez Lopez, S. Goy Lopez, J.M. Hernandez, M.I. Josa, G. Merino, E. Navarro De Martino, J. Puerta Pelayo, A. Quintario Olmeda, I. Redondo, L. Romero, J. Santaolalla, M.S. Soares, C. Willmott

Universidad Autónoma de Madrid, Madrid, Spain
C. Albajar, J.F. de Trocóniz

Universidad de Oviedo, Oviedo, Spain
H. Brun, J. Cuevas, J. Fernandez Menendez, S. Folgueras, I. Gonzalez Caballero, L. Lloret Iglesias, J. Piedra Gomez

Instituto de Física de Cantabria (IFCA), CSIC-Universidad de Cantabria, Santander, Spain
J.A. Brochero Cifuentes, I.J. Cabrillo, A. Calderon, S.H. Chuang, J. Duarte Campderros, M. Fernandez, G. Gomez, J. Gonzalez Sanchez, A. Graziano, C. Jorda, A. Lopez Virto, J. Marco, R. Marco, C. Martinez Rivero, F. Matorras, F.J. Munoz Sanchez, T. Rodrigo, A.Y. Rodríguez-Marrero, A. Ruiz-Jimeno, L. Scodellaro, I. Vila, R. Vilar Cortabitarte

CERN, European Organization for Nuclear Research, Geneva, Switzerland
D. Abbaneo, E. Auffray, G. Auzinger, M. Bachtis, P. Baillon, A.H. Ball, D. Barney, J. Bendavid, J.F. Benitez, C. Bernet[8], G. Bianchi, P. Bloch, A. Bocci, A. Bonato, O. Bondu, C. Botta, H. Breuker, T. Camporesi, G. Cerminara, T. Christiansen, J.A. Coarasa Perez, S. Colafranceschi[34], D. d'Enterria, A. Dabrowski, A. David, A. De Roeck, S. De Visscher, S. Di Guida, M. Dobson, N. Dupont-Sagorin, A. Elliott-Peisert, J. Eugster, W. Funk, G. Georgiou, M. Giffels, D. Gigi, K. Gill, D. Giordano, M. Girone, M. Giunta, F. Glege, R. Gomez-Reino Garrido, S. Gowdy, R. Guida, J. Hammer, M. Hansen, P. Harris, C. Hartl, A. Hinzmann, V. Innocente, P. Janot, E. Karavakis, K. Kousouris, K. Krajczar, P. Lecoq, Y.-J. Lee, C. Lourenço, N. Magini, M. Malberti, L. Malgeri, M. Mannelli, L. Masetti, F. Meijers, S. Mersi, E. Meschi, R. Moser, M. Mulders, P. Musella, E. Nesvold, L. Orsini, E. Palencia Cortezon, E. Perez, L. Perrozzi, A. Petrilli, A. Pfeiffer, M. Pierini, M. Pimiä, D. Piparo, M. Plagge, L. Quertenmont, A. Racz, W. Reece, G. Rolandi[35], M. Rovere, H. Sakulin, F. Santanastasio, C. Schäfer, C. Schwick, I. Segoni, S. Sekmen, A. Sharma, P. Siegrist, P. Silva, M. Simon, P. Sphicas[36], D. Spiga, M. Stoye, A. Tsirou, G.I. Veres[21], J.R. Vlimant, H.K. Wöhri, S.D. Worm[37], W.D. Zeuner

Paul Scherrer Institut, Villigen, Switzerland

W. Bertl, K. Deiters, W. Erdmann, K. Gabathuler, R. Horisberger, Q. Ingram, H.C. Kaestli, S. König, D. Kotlinski, U. Langenegger, D. Renker, T. Rohe

Institute for Particle Physics, ETH Zurich, Zurich, Switzerland
F. Bachmair, L. Bäni, L. Bianchini, P. Bortignon, M.A. Buchmann, B. Casal, N. Chanon, A. Deisher, G. Dissertori, M. Dittmar, M. Donegà, M. Dünser, P. Eller, K. Freudenreich, C. Grab, D. Hits, P. Lecomte, W. Lustermann, B. Mangano, A.C. Marini, P. Martinez Ruiz del Arbol, N. Mohr, F. Moortgat, C. Nägeli[38], P. Nef, F. Nessi-Tedaldi, F. Pandolfi, L. Pape, F. Pauss, M. Peruzzi, F.J. Ronga, M. Rossini, L. Sala, A.K. Sanchez, A. Starodumov[39], B. Stieger, M. Takahashi, L. Tauscher[†], A. Thea, K. Theofilatos, D. Treille, C. Urscheler, R. Wallny, H.A. Weber

Universität Zürich, Zurich, Switzerland
C. Amsler[40], V. Chiochia, C. Favaro, M. Ivova Rikova, B. Kilminster, B. Millan Mejias, P. Otiougova, P. Robmann, H. Snoek, S. Taroni, S. Tupputi, M. Verzetti

National Central University, Chung-Li, Taiwan
M. Cardaci, K.H. Chen, C. Ferro, C.M. Kuo, S.W. Li, W. Lin, Y.J. Lu, R. Volpe, S.S. Yu

National Taiwan University (NTU), Taipei, Taiwan
P. Bartalini, P. Chang, Y.H. Chang, Y.W. Chang, Y. Chao, K.F. Chen, C. Dietz, U. Grundler, W.-S. Hou, Y. Hsiung, K.Y. Kao, Y.J. Lei, R.-S. Lu, D. Majumder, E. Petrakou, X. Shi, J.G. Shiu, Y.M. Tzeng, M. Wang

Chulalongkorn University, Bangkok, Thailand
B. Asavapibhop, N. Suwonjandee

Cukurova University, Adana, Turkey
A. Adiguzel, M.N. Bakirci[41], S. Cerci[42], C. Dozen, I. Dumanoglu, E. Eskut, S. Girgis, G. Gokbulut, E. Gurpinar, I. Hos, E.E. Kangal, A. Kayis Topaksu, G. Onengut[43], K. Ozdemir, S. Ozturk[41], A. Polatoz, K. Sogut[44], D. Sunar Cerci[42], B. Tali[42], H. Topakli[41], M. Vergili

Middle East Technical University, Physics Department, Ankara, Turkey
I.V. Akin, T. Aliev, B. Bilin, S. Bilmis, M. Deniz, H. Gamsizkan, A.M. Guler, G. Karapinar[45], K. Ocalan, A. Ozpineci, M. Serin, R. Sever, U.E. Surat, M. Yalvac, M. Zeyrek

Bogazici University, Istanbul, Turkey
E. Gülmez, B. Isildak[46], M. Kaya[47], O. Kaya[47], S. Ozkorucuklu[48], N. Sonmez[49]

Istanbul Technical University, Istanbul, Turkey
H. Bahtiyar[50], E. Barlas, K. Cankocak, Y.O. Günaydin[51], F.I. Vardarlı, M. Yücel

National Scientific Center, Kharkov Institute of Physics and Technology, Kharkov, Ukraine
L. Levchuk, P. Sorokin

University of Bristol, Bristol, United Kingdom
J.J. Brooke, E. Clement, D. Cussans, H. Flacher, R. Frazier, J. Goldstein, M. Grimes, G.P. Heath, H.F. Heath, L. Kreczko, S. Metson, D.M. Newbold[37], K. Nirunpong, A. Poll, S. Senkin, V.J. Smith, T. Williams

Rutherford Appleton Laboratory, Didcot, United Kingdom
L. Basso[52], K.W. Bell, A. Belyaev[52], C. Brew, R.M. Brown, D.J.A. Cockerill, J.A. Coughlan, K. Harder, S. Harper, J. Jackson, E. Olaiya, D. Petyt, B.C. Radburn-Smith, C.H. Shepherd-Themistocleous, I.R. Tomalin, W.J. Womersley

Imperial College, London, United Kingdom
R. Bainbridge, O. Buchmuller, D. Burton, D. Colling, N. Cripps, M. Cutajar, P. Dauncey, G. Davies, M. Della Negra, W. Ferguson, J. Fulcher, D. Futyan, A. Gilbert, A. Guneratne Bryer, G. Hall, Z. Hatherell, J. Hays, G. Iles, M. Jarvis, G. Karapostoli, M. Kenzie, R. Lane, R. Lucas[37], L. Lyons, A.-M. Magnan, J. Marrouche, B. Mathias, R. Nandi, J. Nash, A. Nikitenko[39], J. Pela, M. Pesaresi, K. Petridis, M. Pioppi[53], D.M. Raymond, S. Rogerson, A. Rose, C. Seez, P. Sharp†, A. Sparrow, A. Tapper, M. Vazquez Acosta, T. Virdee, S. Wakefield, N. Wardle, T. Whyntie

Brunel University, Uxbridge, United Kingdom
M. Chadwick, J.E. Cole, P.R. Hobson, A. Khan, P. Kyberd, D. Leggat, D. Leslie, W. Martin, I.D. Reid, P. Symonds, L. Teodorescu, M. Turner

Baylor University, Waco, USA
J. Dittmann, K. Hatakeyama, A. Kasmi, H. Liu, T. Scarborough

The University of Alabama, Tuscaloosa, USA
O. Charaf, S.I. Cooper, C. Henderson, P. Rumerio

Boston University, Boston, USA
A. Avetisyan, T. Bose, C. Fantasia, A. Heister, P. Lawson, D. Lazic, J. Rohlf, D. Sperka, J. St. John, L. Sulak

Brown University, Providence, USA
J. Alimena, S. Bhattacharya, G. Christopher, D. Cutts, Z. Demiragli, A. Ferapontov, A. Garabedian, U. Heintz, S. Jabeen, G. Kukartsev, E. Laird, G. Landsberg, M. Luk, M. Narain, M. Segala, T. Sinthuprasith, T. Speer

University of California, Davis, Davis, USA
R. Breedon, G. Breto, M. Calderon De La Barca Sanchez, S. Chauhan, M. Chertok, J. Conway, R. Conway, P.T. Cox, R. Erbacher, M. Gardner, R. Houtz, W. Ko, A. Kopecky, R. Lander, O. Mall, T. Miceli, R. Nelson, D. Pellett, F. Ricci-Tam, B. Rutherford, M. Searle, J. Smith, M. Squires, M. Tripathi, S. Wilbur, R. Yohay

University of California, Los Angeles, USA
V. Andreev, D. Cline, R. Cousins, S. Erhan, P. Everaerts, C. Farrell, M. Felcini, J. Hauser, M. Ignatenko, C. Jarvis, G. Rakness, P. Schlein†, E. Takasugi, P. Traczyk, V. Valuev, M. Weber

University of California, Riverside, Riverside, USA
J. Babb, R. Clare, J. Ellison, J.W. Gary, G. Hanson, H. Liu, O.R. Long, A. Luthra, H. Nguyen, S. Paramesvaran, J. Sturdy, S. Sumowidagdo, R. Wilken, S. Wimpenny

University of California, San Diego, La Jolla, USA
W. Andrews, J.G. Branson, G.B. Cerati, S. Cittolin, D. Evans, A. Holzner, R. Kelley, M. Lebourgeois, J. Letts, I. Macneill, S. Padhi, C. Palmer, G. Petrucciani, M. Pieri, M. Sani, V. Sharma, S. Simon, E. Sudano, M. Tadel, Y. Tu, A. Vartak, S. Wasserbaech[54], F. Würthwein, A. Yagil, J. Yoo

University of California, Santa Barbara, Santa Barbara, USA
D. Barge, R. Bellan, C. Campagnari, M. D'Alfonso, T. Danielson, K. Flowers, P. Geffert, C. George, F. Golf, J. Incandela, C. Justus, P. Kalavase, D. Kovalskyi, V. Krutelyov, S. Lowette, R. Magaña Villalba, N. Mccoll, V. Pavlunin, J. Ribnik, J. Richman, R. Rossin, D. Stuart, W. To, C. West

California Institute of Technology, Pasadena, USA
A. Apresyan, A. Bornheim, J. Bunn, Y. Chen, E. Di Marco, J. Duarte, D. Kcira, Y. Ma, A. Mott,

H.B. Newman, C. Rogan, M. Spiropulu, V. Timciuc, J. Veverka, R. Wilkinson, S. Xie, Y. Yang, R.Y. Zhu

Carnegie Mellon University, Pittsburgh, USA
V. Azzolini, A. Calamba, R. Carroll, T. Ferguson, Y. Iiyama, D.W. Jang, Y.F. Liu, M. Paulini, J. Russ, H. Vogel, I. Vorobiev

University of Colorado at Boulder, Boulder, USA
J.P. Cumalat, B.R. Drell, W.T. Ford, A. Gaz, E. Luiggi Lopez, U. Nauenberg, J.G. Smith, K. Stenson, K.A. Ulmer, S.R. Wagner

Cornell University, Ithaca, USA
J. Alexander, A. Chatterjee, N. Eggert, L.K. Gibbons, W. Hopkins, A. Khukhunaishvili, B. Kreis, N. Mirman, G. Nicolas Kaufman, J.R. Patterson, A. Ryd, E. Salvati, W. Sun, W.D. Teo, J. Thom, J. Thompson, J. Tucker, Y. Weng, L. Winstrom, P. Wittich

Fairfield University, Fairfield, USA
D. Winn

Fermi National Accelerator Laboratory, Batavia, USA
S. Abdullin, M. Albrow, J. Anderson, G. Apollinari, L.A.T. Bauerdick, A. Beretvas, J. Berryhill, P.C. Bhat, K. Burkett, J.N. Butler, V. Chetluru, H.W.K. Cheung, F. Chlebana, S. Cihangir, V.D. Elvira, I. Fisk, J. Freeman, Y. Gao, E. Gottschalk, L. Gray, D. Green, O. Gutsche, D. Hare, R.M. Harris, J. Hirschauer, B. Hooberman, S. Jindariani, M. Johnson, U. Joshi, B. Klima, S. Kunori, S. Kwan, J. Linacre, D. Lincoln, R. Lipton, J. Lykken, K. Maeshima, J.M. Marraffino, V.I. Martinez Outschoorn, S. Maruyama, D. Mason, P. McBride, K. Mishra, S. Mrenna, Y. Musienko[55], C. Newman-Holmes, V. O'Dell, O. Prokofyev, N. Ratnikova, E. Sexton-Kennedy, S. Sharma, W.J. Spalding, L. Spiegel, L. Taylor, S. Tkaczyk, N.V. Tran, L. Uplegger, E.W. Vaandering, R. Vidal, J. Whitmore, W. Wu, F. Yang, J.C. Yun

University of Florida, Gainesville, USA
D. Acosta, P. Avery, D. Bourilkov, M. Chen, T. Cheng, S. Das, M. De Gruttola, G.P. Di Giovanni, D. Dobur, A. Drozdetskiy, R.D. Field, M. Fisher, Y. Fu, I.K. Furic, J. Hugon, B. Kim, J. Konigsberg, A. Korytov, A. Kropivnitskaya, T. Kypreos, J.F. Low, K. Matchev, P. Milenovic[56], G. Mitselmakher, L. Muniz, R. Remington, A. Rinkevicius, N. Skhirtladze, M. Snowball, J. Yelton, M. Zakaria

Florida International University, Miami, USA
V. Gaultney, S. Hewamanage, S. Linn, P. Markowitz, G. Martinez, J.L. Rodriguez

Florida State University, Tallahassee, USA
T. Adams, A. Askew, J. Bochenek, J. Chen, B. Diamond, S.V. Gleyzer, J. Haas, S. Hagopian, V. Hagopian, K.F. Johnson, H. Prosper, V. Veeraraghavan, M. Weinberg

Florida Institute of Technology, Melbourne, USA
M.M. Baarmand, B. Dorney, M. Hohlmann, H. Kalakhety, F. Yumiceva

University of Illinois at Chicago (UIC), Chicago, USA
M.R. Adams, L. Apanasevich, V.E. Bazterra, R.R. Betts, I. Bucinskaite, J. Callner, R. Cavanaugh, O. Evdokimov, L. Gauthier, C.E. Gerber, D.J. Hofman, S. Khalatyan, P. Kurt, F. Lacroix, D.H. Moon, C. O'Brien, C. Silkworth, D. Strom, P. Turner, N. Varelas

The University of Iowa, Iowa City, USA
U. Akgun, E.A. Albayrak[50], B. Bilki[57], W. Clarida, K. Dilsiz, F. Duru, S. Griffiths, J.-P. Merlo,

H. Mermerkaya[58], A. Mestvirishvili, A. Moeller, J. Nachtman, C.R. Newsom, H. Ogul, Y. Onel, F. Ozok[50], S. Sen, P. Tan, E. Tiras, J. Wetzel, T. Yetkin[59], K. Yi

Johns Hopkins University, Baltimore, USA
B.A. Barnett, B. Blumenfeld, S. Bolognesi, D. Fehling, G. Giurgiu, A.V. Gritsan, G. Hu, P. Maksimovic, M. Swartz, A. Whitbeck

The University of Kansas, Lawrence, USA
P. Baringer, A. Bean, G. Benelli, R.P. Kenny III, M. Murray, D. Noonan, S. Sanders, R. Stringer, J.S. Wood

Kansas State University, Manhattan, USA
A.F. Barfuss, I. Chakaberia, A. Ivanov, S. Khalil, M. Makouski, Y. Maravin, S. Shrestha, I. Svintradze

Lawrence Livermore National Laboratory, Livermore, USA
J. Gronberg, D. Lange, F. Rebassoo, D. Wright

University of Maryland, College Park, USA
A. Baden, B. Calvert, S.C. Eno, J.A. Gomez, N.J. Hadley, R.G. Kellogg, T. Kolberg, Y. Lu, M. Marionneau, A.C. Mignerey, K. Pedro, A. Peterman, A. Skuja, J. Temple, M.B. Tonjes, S.C. Tonwar

Massachusetts Institute of Technology, Cambridge, USA
A. Apyan, G. Bauer, W. Busza, I.A. Cali, M. Chan, L. Di Matteo, V. Dutta, G. Gomez Ceballos, M. Goncharov, D. Gulhan, Y. Kim, M. Klute, Y.S. Lai, A. Levin, P.D. Luckey, T. Ma, S. Nahn, C. Paus, D. Ralph, C. Roland, G. Roland, G.S.F. Stephans, F. Stöckli, K. Sumorok, D. Velicanu, R. Wolf, B. Wyslouch, M. Yang, Y. Yilmaz, A.S. Yoon, M. Zanetti, V. Zhukova

University of Minnesota, Minneapolis, USA
B. Dahmes, A. De Benedetti, G. Franzoni, A. Gude, J. Haupt, S.C. Kao, K. Klapoetke, Y. Kubota, J. Mans, N. Pastika, R. Rusack, M. Sasseville, A. Singovsky, N. Tambe, J. Turkewitz

University of Mississippi, Oxford, USA
L.M. Cremaldi, R. Kroeger, L. Perera, R. Rahmat, D.A. Sanders, D. Summers

University of Nebraska-Lincoln, Lincoln, USA
E. Avdeeva, K. Bloom, S. Bose, D.R. Claes, A. Dominguez, M. Eads, R. Gonzalez Suarez, J. Keller, I. Kravchenko, J. Lazo-Flores, S. Malik, F. Meier, G.R. Snow

State University of New York at Buffalo, Buffalo, USA
J. Dolen, A. Godshalk, I. Iashvili, S. Jain, A. Kharchilava, A. Kumar, S. Rappoccio, Z. Wan

Northeastern University, Boston, USA
G. Alverson, E. Barberis, D. Baumgartel, M. Chasco, J. Haley, A. Massironi, D. Nash, T. Orimoto, D. Trocino, D. Wood, J. Zhang

Northwestern University, Evanston, USA
A. Anastassov, K.A. Hahn, A. Kubik, L. Lusito, N. Mucia, N. Odell, B. Pollack, A. Pozdnyakov, M. Schmitt, S. Stoynev, K. Sung, M. Velasco, S. Won

University of Notre Dame, Notre Dame, USA
D. Berry, A. Brinkerhoff, K.M. Chan, M. Hildreth, C. Jessop, D.J. Karmgard, J. Kolb, K. Lannon, W. Luo, S. Lynch, N. Marinelli, D.M. Morse, T. Pearson, M. Planer, R. Ruchti, J. Slaunwhite, N. Valls, M. Wayne, M. Wolf

The Ohio State University, Columbus, USA
L. Antonelli, B. Bylsma, L.S. Durkin, C. Hill, R. Hughes, K. Kotov, T.Y. Ling, D. Puigh, M. Rodenburg, G. Smith, C. Vuosalo, G. Williams, B.L. Winer, H. Wolfe

Princeton University, Princeton, USA
E. Berry, P. Elmer, V. Halyo, P. Hebda, J. Hegeman, A. Hunt, P. Jindal, S.A. Koay, P. Lujan, D. Marlow, T. Medvedeva, M. Mooney, J. Olsen, P. Piroué, X. Quan, A. Raval, H. Saka, D. Stickland, C. Tully, J.S. Werner, S.C. Zenz, A. Zuranski

University of Puerto Rico, Mayaguez, USA
E. Brownson, A. Lopez, H. Mendez, J.E. Ramirez Vargas

Purdue University, West Lafayette, USA
E. Alagoz, D. Benedetti, G. Bolla, D. Bortoletto, M. De Mattia, A. Everett, Z. Hu, M. Jones, K. Jung, O. Koybasi, M. Kress, N. Leonardo, D. Lopes Pegna, V. Maroussov, P. Merkel, D.H. Miller, N. Neumeister, I. Shipsey, D. Silvers, A. Svyatkovskiy, M. Vidal Marono, F. Wang, W. Xie, L. Xu, H.D. Yoo, J. Zablocki, Y. Zheng

Purdue University Calumet, Hammond, USA
S. Guragain, N. Parashar

Rice University, Houston, USA
A. Adair, B. Akgun, K.M. Ecklund, F.J.M. Geurts, W. Li, B.P. Padley, R. Redjimi, J. Roberts, J. Zabel

University of Rochester, Rochester, USA
B. Betchart, A. Bodek, R. Covarelli, P. de Barbaro, R. Demina, Y. Eshaq, T. Ferbel, A. Garcia-Bellido, P. Goldenzweig, J. Han, A. Harel, D.C. Miner, G. Petrillo, D. Vishnevskiy, M. Zielinski

The Rockefeller University, New York, USA
A. Bhatti, R. Ciesielski, L. Demortier, K. Goulianos, G. Lungu, S. Malik, C. Mesropian

Rutgers, The State University of New Jersey, Piscataway, USA
S. Arora, A. Barker, J.P. Chou, C. Contreras-Campana, E. Contreras-Campana, D. Duggan, D. Ferencek, Y. Gershtein, R. Gray, E. Halkiadakis, D. Hidas, A. Lath, S. Panwalkar, M. Park, R. Patel, V. Rekovic, J. Robles, S. Salur, S. Schnetzer, C. Seitz, S. Somalwar, R. Stone, S. Thomas, M. Walker

University of Tennessee, Knoxville, USA
G. Cerizza, M. Hollingsworth, K. Rose, S. Spanier, Z.C. Yang, A. York

Texas A&M University, College Station, USA
O. Bouhali[60], R. Eusebi, W. Flanagan, J. Gilmore, T. Kamon[61], V. Khotilovich, R. Montalvo, I. Osipenkov, Y. Pakhotin, A. Perloff, J. Roe, A. Safonov, T. Sakuma, I. Suarez, A. Tatarinov, D. Toback

Texas Tech University, Lubbock, USA
N. Akchurin, J. Damgov, C. Dragoiu, P.R. Dudero, C. Jeong, K. Kovitanggoon, S.W. Lee, T. Libeiro, I. Volobouev

Vanderbilt University, Nashville, USA
E. Appelt, A.G. Delannoy, S. Greene, A. Gurrola, W. Johns, C. Maguire, Y. Mao, A. Melo, M. Sharma, P. Sheldon, B. Snook, S. Tuo, J. Velkovska

University of Virginia, Charlottesville, USA
M.W. Arenton, S. Boutle, B. Cox, B. Francis, J. Goodell, R. Hirosky, A. Ledovskoy, C. Lin, C. Neu, J. Wood

Wayne State University, Detroit, USA
S. Gollapinni, R. Harr, P.E. Karchin, C. Kottachchi Kankanamge Don, P. Lamichhane, A. Sakharov

University of Wisconsin, Madison, USA
D.A. Belknap, L. Borrello, D. Carlsmith, M. Cepeda, S. Dasu, E. Friis, M. Grothe, R. Hall-Wilton, M. Herndon, A. Hervé, K. Kaadze, P. Klabbers, J. Klukas, A. Lanaro, R. Loveless, A. Mohapatra, M.U. Mozer, I. Ojalvo, G.A. Pierro, G. Polese, I. Ross, A. Savin, W.H. Smith, J. Swanson

†: Deceased
1: Also at Vienna University of Technology, Vienna, Austria
2: Also at CERN, European Organization for Nuclear Research, Geneva, Switzerland
3: Also at Institut Pluridisciplinaire Hubert Curien, Université de Strasbourg, Université de Haute Alsace Mulhouse, CNRS/IN2P3, Strasbourg, France
4: Also at National Institute of Chemical Physics and Biophysics, Tallinn, Estonia
5: Also at Skobeltsyn Institute of Nuclear Physics, Lomonosov Moscow State University, Moscow, Russia
6: Also at Universidade Estadual de Campinas, Campinas, Brazil
7: Also at California Institute of Technology, Pasadena, USA
8: Also at Laboratoire Leprince-Ringuet, Ecole Polytechnique, IN2P3-CNRS, Palaiseau, France
9: Also at Zewail City of Science and Technology, Zewail, Egypt
10: Also at Suez Canal University, Suez, Egypt
11: Also at Cairo University, Cairo, Egypt
12: Also at Fayoum University, El-Fayoum, Egypt
13: Also at British University in Egypt, Cairo, Egypt
14: Now at Ain Shams University, Cairo, Egypt
15: Also at National Centre for Nuclear Research, Swierk, Poland
16: Also at Université de Haute Alsace, Mulhouse, France
17: Also at Joint Institute for Nuclear Research, Dubna, Russia
18: Also at Brandenburg University of Technology, Cottbus, Germany
19: Also at The University of Kansas, Lawrence, USA
20: Also at Institute of Nuclear Research ATOMKI, Debrecen, Hungary
21: Also at Eötvös Loránd University, Budapest, Hungary
22: Also at Tata Institute of Fundamental Research - EHEP, Mumbai, India
23: Also at Tata Institute of Fundamental Research - HECR, Mumbai, India
24: Now at King Abdulaziz University, Jeddah, Saudi Arabia
25: Also at University of Visva-Bharati, Santiniketan, India
26: Also at University of Ruhuna, Matara, Sri Lanka
27: Also at Isfahan University of Technology, Isfahan, Iran
28: Also at Sharif University of Technology, Tehran, Iran
29: Also at Plasma Physics Research Center, Science and Research Branch, Islamic Azad University, Tehran, Iran
30: Also at Università degli Studi di Siena, Siena, Italy
31: Also at Purdue University, West Lafayette, USA
32: Also at Universidad Michoacana de San Nicolas de Hidalgo, Morelia, Mexico
33: Also at Faculty of Physics, University of Belgrade, Belgrade, Serbia
34: Also at Facoltà Ingegneria, Università di Roma, Roma, Italy

35: Also at Scuola Normale e Sezione dell'INFN, Pisa, Italy
36: Also at University of Athens, Athens, Greece
37: Also at Rutherford Appleton Laboratory, Didcot, United Kingdom
38: Also at Paul Scherrer Institut, Villigen, Switzerland
39: Also at Institute for Theoretical and Experimental Physics, Moscow, Russia
40: Also at Albert Einstein Center for Fundamental Physics, Bern, Switzerland
41: Also at Gaziosmanpasa University, Tokat, Turkey
42: Also at Adiyaman University, Adiyaman, Turkey
43: Also at Cag University, Mersin, Turkey
44: Also at Mersin University, Mersin, Turkey
45: Also at Izmir Institute of Technology, Izmir, Turkey
46: Also at Ozyegin University, Istanbul, Turkey
47: Also at Kafkas University, Kars, Turkey
48: Also at Suleyman Demirel University, Isparta, Turkey
49: Also at Ege University, Izmir, Turkey
50: Also at Mimar Sinan University, Istanbul, Istanbul, Turkey
51: Also at Kahramanmaras Sütcü Imam University, Kahramanmaras, Turkey
52: Also at School of Physics and Astronomy, University of Southampton, Southampton, United Kingdom
53: Also at INFN Sezione di Perugia; Università di Perugia, Perugia, Italy
54: Also at Utah Valley University, Orem, USA
55: Also at Institute for Nuclear Research, Moscow, Russia
56: Also at University of Belgrade, Faculty of Physics and Vinca Institute of Nuclear Sciences, Belgrade, Serbia
57: Also at Argonne National Laboratory, Argonne, USA
58: Also at Erzincan University, Erzincan, Turkey
59: Also at Yildiz Technical University, Istanbul, Turkey
60: Also at Texas A&M University at Qatar, Doha, Qatar
61: Also at Kyungpook National University, Daegu, Korea